

Ensuring DNN Solution Feasibility for Optimization Problems with Convex Constraints and Its Application to DC Optimal Power Flow Problems

Tianyu Zhao, Xiang Pan, Minghua Chen, and Steven H. Low

Abstract

Ensuring solution feasibility is a key challenge in developing Deep Neural Network (DNN) schemes for solving constrained optimization problems, due to inherent DNN prediction errors. In this paper, we propose a “preventive learning” framework to systematically guarantee DNN solution feasibility for problems with convex constraints and general objective functions. We first apply a predict-and-reconstruct design to not only guarantee equality constraints but also exploit them to reduce the number of variables to be predicted by DNN. Then, as a key methodological contribution, we systematically calibrate inequality constraints used in DNN training, thereby anticipating prediction errors and ensuring the resulting solutions remain feasible. We characterize the calibration magnitudes and the DNN size sufficient for ensuring universal feasibility. We propose a new *Adversary-Sample Aware* training algorithm to improve DNN’s optimality performance without sacrificing feasibility guarantee. Overall, the framework provides two DNNs. The first one from characterizing the sufficient DNN size can guarantee universal feasibility while the other from the proposed training algorithm further improves optimality and maintains DNN’s universal feasibility simultaneously. We apply the preventive learning framework to develop **DeepOPF+** for solving the essential DC optimal power flow problem in grid operation. It improves over existing DNN-based schemes in ensuring feasibility and attaining consistent desirable speedup performance in both light-load and heavy-load regimes. Simulation results over IEEE Case-30/118/300 test cases show that **DeepOPF+** generates 100% feasible solutions with <0.5% optimality loss and up to two orders of magnitude computational speedup, as compared to a state-of-the-art iterative solver.

I. INTRODUCTION

Recently, there have been increasing interests in developing neural network schemes, including those based on deep neural networks (DNN), to solve constrained optimization problems in various problem domains, especially those needed to be solved repeatedly in real-time. The idea behind these machine learning approaches is to leverage the universal approximation capability of DNNs [1]–[3] to learn the mapping between the input parameters to the

Tianyu Zhao and Xiang Pan are with Information Engineering, The Chinese University of Hong Kong. Minghua Chen is with School of Data Science, City University of Hong Kong. Steven H. Low is with Department of Computing and Mathematical Sciences, California Institute of Technology.

solution of an optimization problem. Then one can directly pass the input parameters through the trained neural network to obtain a quality solution much faster than iterative solvers. For example, researchers have developed DNN schemes to solve the essential optimal power flow problems in grid operation with sub-percentage optimality loss and several order of magnitude speedup as compared to conventional solvers, for power networks with more than two thousand buses [4]–[10]. Similarly, DNN-based schemes also obtain desirable results for real-time power control and beam-forming designs [11], [12] problems in wireless communication systems in a fraction of the time used by existing solvers.

Despite of these promising results, however, a major criticism of DNN and machine learning schemes is that they usually cannot guarantee the solution feasibility with respect to all the inequality and equality constraints of the optimization problem [5]. This is due to the inherent prediction errors of neural network models. Failing to respect the system physical and operational constraints can be fatal and lead to system instability or incur higher operating cost for the system operator [13]. Existing works address the feasibility concern mainly by incorporating the constraints violation (e.g., a penalty function of the dual variables corresponding to the constraints) into the loss function to guide the neural network training. These endeavors, while generating great insights to the DNN design and working to some extent in case studies, may not guarantee the solution feasibility without resorting to an expensive post-processing procedure, e.g., feeding the DNN solution as a warm start point into a conventional solver to obtain a feasible final solution. See Sec. II for detail discussions on the related works. To date, it remains a largely open issue of ensuring DNN solution feasibility for constrained optimization problems.

In this paper, we address this issue for Optimization Problems with Convex Constraints (OPCC) and general objective functions. Our idea is to characterize the room for (prediction) errors without violating the constraints, and then train a properly designed DNN in a preventive manner to ensure the resulting DNN solutions remain feasible even with prediction errors, thus avoiding the need to go through an expensive post-processing procedure. We make the following contributions:

- After formulating the OPCC problem in Sec. III, we propose a “preventive learning” framework to ensure the DNN solution feasibility for OPCC in Sec. IV. We first apply the predict-and-reconstruct design [5] to not only guarantee equality constraints but also exploit them to reduce the number of variables to be predicted by DNN. Then we systematically calibrate inequality constraints used in DNN training, thereby anticipating prediction errors and ensuring the resulting DNN solutions remain feasible.
- Then in Sec. IV-B, we characterize the calibration magnitudes necessary for ensuring universal feasibility with respect to the entire parameter input region by solving a bi-level problem with a heuristic method. We then derive the sufficient DNN size in ensuring universal feasibility in Sec. IV-C, by adapting an integer linear formulation from [14], [15]. In Sec. IV-D, based on the ideas of active training and adversarial training, we propose a new *Adversary-Sample Aware* training algorithm to improve DNN’s optimality performance without sacrificing feasibility guarantee. Overall, the framework provides two DNNs. The first one from characterizing the sufficient DNN size can guarantee universal feasibility while the other from the proposed training algorithm further improves optimality and maintains DNN’s universal feasibility simultaneously.
- In Sec. V, we apply the framework to design a DNN scheme, DeepOPF+, for solving DC optimal power

flow (DC-OPF) problems in grid operation. It improves over existing DNN schemes in ensuring feasibility and attaining consistent desirable speedup performance in both light-load and heavy-load regimes. Note that under the heavy-load regime, the systems constraints are highly binding and the existing DNN schemes may not achieve high speedups due to the need of an expensive post-processing procedure to recover feasibility of infeasible DNN solutions. Simulation results over IEEE Case-30/118/300 test cases show that DeepOPF+ generates 100% feasible solutions with at most $<0.5\%$ optimality loss and two orders of magnitude computational speedup as compared to a state-of-the-art iteration-based solver.

II. RELATED WORK

Machine learning, including DNNs, has been applied to challenging constrained optimization for decades [16]–[18]. For brevity, we focus on applying learning-based methods to solve constrained optimization problems, divided into two categories.

The first category is the hybrid approach. It integrates learning techniques to facilitate conventional algorithms solving challenging constrained optimization problems [19]–[28]. For example, some works use DNN to identify the active/inactive constraints of LP/QP to reduce problem size [29]–[33] or predict warm-start initial points or gradients to accelerate the solving process [34], [35] and speed up the branch-and-bound algorithm [36], [37]. Nevertheless, the core of these methods is still conventional solver that may incur high computational costs for large-scale programs due to the inevitable iteration process.

The second category is the stand-alone approach, which leverages machine learning models to predict constrained optimization problems solutions without resorting to the conventional solver [4], [5], [38]–[42]. For example, existing works belong to the “learn to optimize” field, using RNN to mimic the gradient descent-wise iteration and achieve faster convergence speed empirically [43], [44]. Other works like [6], [7], [13] directly used the DNN model to predict the final solution (regarded as end-to-end method), which can further reduce the computing time compared to the iteration-based approaches. These approaches, in general, can have better speedup performance compared with the hybrid approaches.

Though end-to-end methods have been actively studied for constrained optimizations with promising speedups, the lack of feasibility guarantees presents a fundamental barrier for practical application, e.g., infeasibility due to inaccurate active/inactive limits identification. Infeasible solutions from the end-to-end approach are also observed [5], [13], especially considering the DNN worst-case performance under adversary input with serious constraints violations [14], [45], [46]. This echoes the critical challenge of ensuring the DNN solutions feasibility.

Some efforts have been put to improve DNN feasibility, e.g., considering solution generalization [47] or appealing to post-processing schemes [5]. While the projection based post-processing step can retrieve a feasible solution in the face of infeasibility, the scheme turns to be computationally expensive and inefficient. Several techniques that incorporate problem constraints during training to improve DNN feasibility are proposed [6], [7]. These approaches enforce equality constraints by predicting a set of variables and recovering the remaining ones from such equality equations. Though the inequality limits are considered as penalty during training, the DNN solution could still be infeasible due to approximation errors. In [45], [46], the Physics-Informed Neural Networks (PINNs) are

applied to predict the optimization problem solutions while incorporating the problem Karush–Kuhn–Tucker (KKT) conditions during training. Though the PINNs present better worst-case performance, the constraints satisfaction is not guaranteed by the obtained DNN solution. There is an emerging line of works focusing on developing structured neural network layers that specify the implicit relationships between inputs and outputs [48]–[57]. Such approaches can directly enforce constraints, e.g., by projecting neural network outputs onto the feasible region described by linear constraints using quadratic programming layers [58], or convex optimization layers [59] for general convex constraints. However, such implicit optimization layers tend to be computational expense and lead these projection-based schemes inefficient. Our work also fundamentally relates to the field of DNN robustness. Several methods have been proposed to verify DNN robustness against input adversarial perturbations for classification tasks [60]–[63]. These approaches generally depends on the network relaxation with accuracy as the metric. Our work differs significantly from the one in [13] in that our framework provides some fundamental understanding in ensuring DNN solution feasibility for optimization problems, including determining both the inequality constraint calibration magnitude and DNN size necessary for ensuring universal feasibility and deriving the active training scheme considering both optimality and feasibility.

To our best knowledge, our work is the first to provide systematical understanding whether it is possible to achieve DNN solution's universal feasibility for all the inputs within an interested region, and if so, how to design and train a DNN to achieve decent optimality performance while ensuring solution feasibility.

III. OPTIMIZATION PROBLEMS WITH CONVEX CONSTRAINTS

We focus on the OPCC formulated as follows [64], [65]:

$$\min_{\mathbf{x} \in \mathcal{R}^N} f(\mathbf{x}, \boldsymbol{\theta}) \quad (1)$$

$$\text{s.t. } a_i^T \mathbf{x} = b_i + c_i^T \boldsymbol{\theta}, \quad i = 1, \dots, p, \quad (2)$$

$$g_j(\mathbf{x}, \boldsymbol{\theta}) \leq e_j, \quad j = 1, \dots, m. \quad (3)$$

$$\underline{x}_k \leq x_k \leq \bar{x}_k, \quad k \in \mathcal{P}. \quad (4)$$

In the formulation, $\mathbf{x} \in \mathcal{R}^N$ are the decision variables and $\boldsymbol{\theta} \in \mathcal{D}$ are the input parameters. The objective function $f(\mathbf{x}, \boldsymbol{\theta})$ is general and can be either convex or non-convex.

We assume the input domain $\mathcal{D} = \{\boldsymbol{\theta} \in \mathcal{R}^M \mid \mathbf{A}_{\boldsymbol{\theta}} \boldsymbol{\theta} \leq \mathbf{b}_{\boldsymbol{\theta}}\}$ is a convex polytope specified by matrix $\mathbf{A}_{\boldsymbol{\theta}}$ and vector $\mathbf{b}_{\boldsymbol{\theta}}$ such that for each $\boldsymbol{\theta} \in \mathcal{D}$, the OPCC in (1)–(4) admits a unique optimal solution. $a_i \in \mathcal{R}^N, b_i \in \mathcal{R}, c_i \in \mathcal{R}^M$ are the coefficients of the equality constraints, $g_j : \mathcal{R}^N \times \mathcal{R}^M \rightarrow \mathcal{R}, j = 1, \dots, m$ are convex functions w.r.t. \mathbf{x} . We use \mathcal{E} to denote the set of inequality constraints. Here we assume the above OPCC (1)–(4) is not over-determined, i.e., the number of equality constraints p does not exceed the decision variable dimension N ($p \leq N$). Hence, given $N - p$ entries of \mathbf{x} , the remaining p variables can generally be determined by these p linear equations. We use \mathcal{P} to denote the set of these $N - p$ variables. We also formulate each $x_k \in \mathcal{P}$ to be restricted by an upper bound \bar{x}_k and lower bound \underline{x}_k (box constraints). Here we focus on the setting that all the inequality constraints g_j are critical. Formally, the critical inequality constraint is defined as

Definition 1. An inequality constraints $g_j(\mathbf{x}, \boldsymbol{\theta})$ is critical if there exists one $\boldsymbol{\theta} \in \mathcal{D}$ and \mathbf{x} satisfying (4) such that (2) hold and $g_j(\mathbf{x}, \boldsymbol{\theta}) > e_j$.

Non-critical constraints are always respected for any combination of input $\boldsymbol{\theta} \in \mathcal{D}$ and \mathbf{x} satisfying (2) and the box constraints (4). Thus removing them will not change the optimal solutions of OPCC for any input parameter in the input domain. Thus without loss of generality, we assume that all the inequality constraints g_j are critical. We refer to Appendix A for the problem formulations with potential non-critical inequality constraints and a method to identify and remove these non-critical inequality constraints as well as the corresponding discussions.

Numerical solvers based on, e.g., interior-point methods [66], can be applied to obtain a solution for OPCC. However, the corresponding time complexity can be significant and limits their applications in practice, especially for large-scale instances. As a concrete example, a critical problem in power system operation, the security-constrained DC-OPF (SC-DCOPF) problem incurs a complexity of $\mathcal{O}(K^{12})$ to solve it optimally, where K is number of buses, limiting its practicability.

The observation that opens the door for DNN scheme development lies in that solving OPCC is equivalent to learning the mapping between input $\boldsymbol{\theta}$ to the optimal solution $\mathbf{x}^*(\boldsymbol{\theta})$, which is continuous w.r.t. $\boldsymbol{\theta}$ if OPCC admits a unique optimal solution for every $\boldsymbol{\theta} \in \mathcal{D}$ [6], [67]. For multiparametric quadratic programs (mp-QP), i.e., f is quadratic w.r.t. \mathbf{x} and g_i are linear functions, $\mathbf{x}^*(\boldsymbol{\theta})$ can be further characterize to be piece-wise linear [65].

As such, it is conceivable to leverage the universal approximation capability of deep feed-forward neural networks [68], to learn the input-solution mapping $\mathbf{x}^*(\boldsymbol{\theta})$ for a given OPCC formulation, and then apply the mapping to obtain optimal solutions for any $\boldsymbol{\theta} \in \mathcal{D}$ in a fraction of the time used by conventional solvers. For example, DNN schemes have been proposed to solve the above-mentioned SC-DCOPF problems with a complexity as low as $\mathcal{O}(K^5)$ and minor optimality loss [5], [6]. See Sec. II for more discussions on developing DNN schemes for solving optimization problems.

While achieving promising speedup and optimality performance, a key challenge in developing DNN approaches for solving constrained optimization problems lies in ensuring solution feasibility, which is nontrivial due to inherent DNN prediction errors. For example, in the previous work [5], [6], the obtained DNN solutions may violate the inequality constraints especially when the constraints are binding. In the following, we propose a preventive learning framework to tackle this issue for designing DNN schemes to solve OPCC.

IV. PREVENTIVE LEARNING FRAMEWORK FOR OPCC

A. Overview of the Framework

We propose a DNN-based preventive framework to solve OPCC by learning input-solution mapping, as depicted in Fig. 1. The framework first adopts the predict-and-reconstruct idea [6], [7], [13] to guarantee the equality constraints satisfaction by predicting a subset of $N - p$ variables in \mathcal{P} and recovering the remaining p ones by solving the linear equations in (2). This way, we not only guarantee equality constraints but also exploit them to reduce the number of variables to be predicted by DNN.

Then as a key component of the proposed framework, we *calibrate* the inequality constraints such that for any interested input parameter, the trained DNN can provide a feasible and close-to-optimal solution even with the

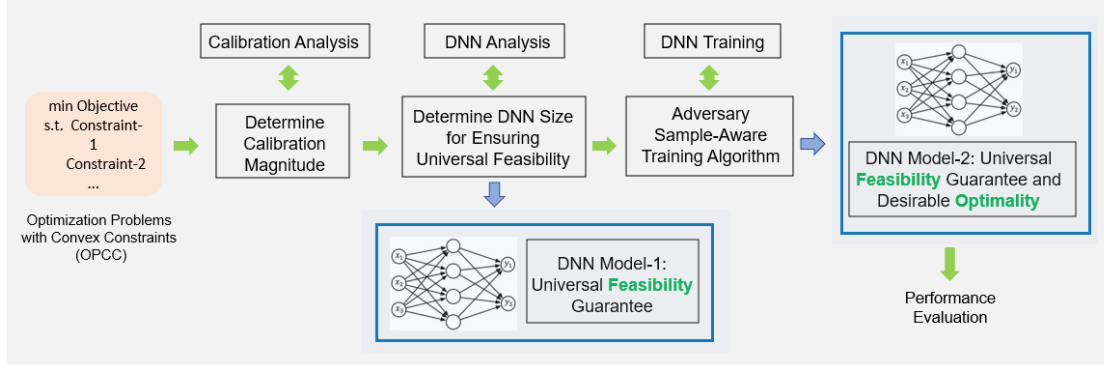


Fig. 1. Overview of preventive learning framework for solving OPCC. The appropriate calibration magnitude is first characterized to preserve the input domain. The sufficient DNN size in guaranteeing universal feasibility is then investigated. The new *Adversary Sample-Aware* training algorithm is applied to train the DNN for desirable optimality performance while ensuring universal feasibility guarantee. DNN Model-1 and DNN Model-2 denote the two different DNNs obtained from the second and third steps respectively.

approximation error. In particular, we calibrate each inequality constraint $g_j(\mathbf{x}, \boldsymbol{\theta}) \leq e_j$ by an appropriate magnitude during the input sampling:

$$g_j(\mathbf{x}, \boldsymbol{\theta}) \leq e_j \times (1_{e_j \geq 0}(1 - \eta_j) + 1_{e_j < 0}(1 + \eta_j)) = \hat{e}_j, \quad \forall j \in \mathcal{E}. \quad (5)$$

Here $\eta_j \in [0, 1]$ denotes the calibration rate.¹ Then, we train the DNN on a (algorithmic designed) dataset created with calibrated limits to learn the corresponding input-solution mapping ($\Omega : \boldsymbol{\theta} \mapsto \mathcal{S}$) and evaluate its performance on a test data-set with the original limits. Thus, even with the inherent prediction error of DNN, the obtained solution can still remain feasible. We remark that during the training stage, only the inequality limits calibration does not reduce the feasibility region of inputs $\boldsymbol{\theta}$ is in consideration. Also, we note that the constraints calibration could lead to the (sub)optimal solutions that are interior points within the original feasible region (the inequality constraints are expected to be not binding) when approximating the input-solution mapping for the OPCC with calibrated constraints. Thus, determine a proper η_j is important. As the approximation capability depends on the size of DNN, another critical problem is to designing DNN with sufficient size for ensuring universal feasibility on the entire parameter input region. In the following subsections, we discuss how to address these problems with a proposed systematic scheme, which consists of three steps:

- First, we describe how determine the appropriate calibration magnitude on the critical inequality constraints to preserve the targeted input region in Sec. IV-B.

¹Another intuitive calibration method is to keep the mean of the (calibrated) upper bound and lower bound of the constraint unchanged. That is, $(\hat{e}_j^u + \hat{e}_j^l)/2$ is the same as the one before calibration, where \hat{e}_j^u and \hat{e}_j^l denote the upper/lower bounds after calibration. We remark that such method 1) may not be applicable to the constraints with only one single unilateral bound, and 2) it introduces additional calibration requirements on the constraints limits compared with the one in (5), which could cause some constraints to have small and conservative calibration magnitude while it can indeed be further calibrated. We refer to Sec. IV-B and Appendix A for the discussion on determining the calibration magnitude.

- Second, as discussed in Sec. IV-C, we show how to determine sufficient size for DNN to obtain universal feasibility across the input region by investigating its approximation capability.
- Third, as presented in Sec. IV-D, we propose a new *Adversary Sample-Aware* algorithm to train a DNN based on the calibrated constraints for achieving desirable optimality and feasibility performance.

Overall, the framework provides two DNNs. The first one from determining the sufficient DNN size can guarantee universal feasibility while the other from the proposed training algorithm further improves optimality without sacrificing DNN's universal feasibility simultaneously. To better deliver the results in the framework, we briefly summarize the relationship between the settings and the applied methodologies in Table I. We further discuss the results that can be obtained in polynomial time by solving the proposed programs.

TABLE I
METHODOLOGIES UNDER DIFFERENT SETTINGS.

Problem setting	Determine calibration magnitude	Determine DNN size for ensuring universal feasibility	ASA training algorithm
General OPCC	*Non-convex optimization	*Bi-level non-convex mixed-integer optimization	*Non-convex mixed-integer optimization
OPLC	[^] Mixed-integer linear programming	[^] Bi-level mixed-integer linear programming	[^] Mixed-integer linear programming

* Symbol * represents that we can obtain a valid bound in polynomial time by solving the corresponding program, which is still be useful for analysis.

* Symbol [^] represents that we may not obtain a valid and useful bound in polynomial time by solving the corresponding program for further analysis.

We remark that the involved problems for each step are indeed non-convex programs. The existing solvers, e.g., Gurobi, CPLEX, or APOPT, may not provide the global optimum. However, we may still be able to obtain the useful bounds from the solver under the specific setting. We briefly present the results in the following, in which the upper/lower bounds denote the (sub-optimal) objective values of the programs that can be obtained in polynomial time, e.g., when the solvers terminate at any time but not returning an optimal solution.

For general OPCC:

- Determine calibration magnitude: We can get a upper bound on the global optimum of the maximum calibration magnitude (with the feasible (sub-optimal) solution), which may not be valid and useful for further analysis. Such an upper bound may lead some input to be infeasible and hence universal feasibility may not be guaranteed.
- Determine DNN size for ensuring universal feasibility: We can get a lower bound (with the feasible (sub-optimal) solution) on the worst-case violation with the obtained DNN parameters while we may not get the valid and useful result of the global optimum of the bi-level program for further analysis. Such determined

DNN size may not guarantee universal feasibility with the obtained objective value under the specified DNN parameters.

- Adversary sample-aware training algorithm: We can get a lower bound on the global optimum of the worst-case violation (with the feasible (sub-optimal) solution), which may not be valid for further analysis. Such a lower bound may not guarantee universal feasibility under the trained DNN.

For Optimization Problems with Linear Constraints (OPLC), i.e., g_j are all linear, $\forall j = 1, \dots, m$:

- Determine calibration magnitude: We can get a *valid lower bound* on the global optimum of the maximum calibration magnitude (may or may not be with the feasible solution). Such a lower bound ensures that we will not calibrate the constraints too much and hence preserves the input parameter region, which is still useful for further analysis in the following steps.
- Determine DNN size for ensuring universal feasibility: We can get a *valid upper bound* on the worst-case violation with the obtained DNN parameters (may or may not be with the feasible solution) and the global optimum of the bi-level MILP program. If such an upper bound is no greater than the calibration magnitude, the determined DNN size is assured to be sufficient and universal feasibility of DNN is guaranteed.
- Adversary sample-aware training algorithm: We can get a *valid upper bound* on the global optimum of the worst-case violation (may or may not be with the feasible solution), which is still useful for analysis. If such an upper bound is no greater than the calibration magnitude, the universal feasibility guarantee of the obtained DNN is assured.

We remark that the bounds obtained from the setting of OPLC can still be useful and valid for further analysis. However, the results under the general OPCC can be loose and may not be utilized with desired performance guarantee. In addition, we state that for each involved program, we can always obtain a feasible (sub-optimal) solution for further use. These results are discussed in the corresponding parts in the paper.

B. Inequality Constraint Calibration Magnitude

We first discuss how to derive the maximum calibration magnitude allowed for the critical inequality constraints, without shrinking the parameter input region. Recall that in the framework, the DNN is trained on the samples from OPCC with calibrated critical constraints as discussed in Sec. IV-A.² However, if we adjust the limits too much, some input $\theta \in \mathcal{D}$ will become infeasible under the calibrated constraints and hence lead to invalid training data with poor generalization, though they are feasible for the original limits. Therefore, it is essential to determine the appropriate calibration range without shrinking the parameter input region \mathcal{D} . We propose the following bi-level

²The non-critical constraints are always respected for any input $\theta \in \mathcal{D}$ and x in the solution space. Hence, calibrating those constraints may only cause higher optimality loss since the reference sub-optimal solutions of OPCC with such calibrations could have larger deviations from the ones under the original setting.

optimization program to study such desired range:

$$\min_{\boldsymbol{\theta}} \max_{x_i, i \in \mathcal{P}} \nu^c \quad (6)$$

$$\text{s.t. } (2) - (4), \quad \boldsymbol{\theta} \in \mathcal{D},$$

$$\nu^c = \min\left\{\frac{e_j - g_j(\boldsymbol{\theta}, \mathbf{x})}{|e_j|}, j \in \mathcal{E}\right\}. \quad (7)$$

Constraints (2)-(4) denote the feasibility of \mathbf{x} with respect to the associated input $\boldsymbol{\theta} \in \mathcal{D}$. Consider the inner maximization problem, the objective finds the maximum of the element-wise least redundancy of the inequality constraints, which is the largest possible constraints calibration rate at each given $\boldsymbol{\theta}$. Note that we only need to calibrate the constraints in \mathcal{E} . The outer minimization problem hence finds the largest possible calibration rate among all $\boldsymbol{\theta} \in \mathcal{D}$, and correspondingly, the supported input feasible region is not reduced. We remark that the inner maximization problem can be reformulated as an convex optimization program by introducing a slack variable λ and a set of convex constraints, such that $\lambda \leq \frac{e_j - g_j(\boldsymbol{\theta}, \mathbf{x})}{|e_j|}, \forall j \in \mathcal{E}$ and maximizing over λ . Though the inner problem is a convex optimization problem (convex constrained with linear objective), the bi-level program (6)-(7) is challenging to solve [69], [70]. In the following Sec. IV-B1 and Sec. IV-B2, we propose an applicable technique to reformulate the bi-level program utilizing the problem characteristic and discuss the optimality and the complexity of the problem.

1) *Techniques for the Bi-Level Program and Maximum Calibration Magnitude.*: Here several techniques can be applied to such bi-level problems. In the following, we adopt the standard approach to reformulated bi-level program to single level by replacing the inner-level problem by its Karush-Kuhn-Tucker (KKT) conditions.³ This yields a single-level mathematical program with complementarity constraints (MPCCs). In particular, the approach contains the following two steps:

- First, replace the inner program by its sufficient and necessary KKT conditions [64].
- Next, incorporate the KKT conditions into the upper-level program as constraints, representing the optimality of the inner maximization in \mathbf{x} .

After solving (6)-(7), we derive the maximum calibration rate, denoted as Δ . We have the following lemma highlighting the appropriate constraints calibration rate without shrinking the original input feasible region \mathcal{D} , considering $\eta_j = \eta, \forall j \in \mathcal{E}$ in (5).

Lemma 1. *If the calibration rate of the inequality constraints calibration satisfies $\eta \leq \Delta$, then any input $\boldsymbol{\theta} \in \mathcal{D}$ is feasible, i.e., for any $\boldsymbol{\theta} \in \mathcal{D}$ there exist a feasible \mathbf{x} such that (2), (4), (5) hold.*

We remark that the obtained uniform calibration rate on each critical constraints forms the *outer bound* of the minimal supporting calibration region defined as follows:

³We always assume Slater's condition hold. Otherwise for some $\boldsymbol{\theta}$, the calibration rate turns to be zero.

Definition 2. The minimal supporting calibration region is defined as the set of calibration magnitude $\{\{\eta_j\}_{j \in \mathcal{E}} | s.t. (2), (4), (5) \text{ hold}\}$. Meanwhile, there exist a $\theta \in \mathcal{D}$ and there does not exist an x such that (2), (4), (5) hold under $\{\{\eta_j + \delta_j\}_{j \in \mathcal{E}}\}$ for any $\delta_j \geq 0$ and at least one $\delta_j > 0$.

The minimal supporting calibration region describes the set of maximal calibration magnitude such that 1) the input parameter region is maintained, and 2) any further calibration on the constraints will lead some input to be infeasible. We remark that such minimal supporting calibration region is not unique, see Appendix A for an example and the approach to obtain (one of) such minimal supporting calibration region. In this work, we consider the uniform calibration rate Δ for further analysis.⁴

Note that the reformulated problem (6)-(7) is indeed in general, still a non-convex optimization problem after such KKT replacement. Existing solvers, e.g., Gurobi, CPLEX, or APOPT, may not generate the global optimal solution for the problem (6)-(7) due to the challenging nature of itself. In the following, we present that for the special class of OPLC, e.g., mp-QP, which is also common in practice, we can improve the results by obtaining a useful lower bound.

2) *Special Case: OPLC:* We remark that for the OPLC, i.e., g_j are all linear, $\forall j = 1, \dots, m$, the reformulated bi-level problem is indeed in the form of quadratically constrained program due to the complementary slackness requirements in the KKT conditions. As the input domain \mathcal{D} is a convex polytope, such quadratically constrained program can be cast as the mixed-integer linear programming (MILP). See Appendix A for the reformulation. If the MILP is solved to zero optimality gap, i.e., exact bound with global optimality, then we obtain the provable maximum calibration rate. If the MILP is solved to a non-zero optimality gap, then we obtain a lower bound on the maximum calibration rate Δ . Such a lower bound guarantees that we will not calibrate the constraints over the allowable limits such that the OPCC with calibrated constraints admits a feasible optimal solution for each input θ in the interested parameter input region \mathcal{D} .⁵ In practice, one may use a smaller calibration compared with the obtain Δ . We can still use the obtained lower bound to determine the sufficient DNN size for universal feasibility and design the *Adversary Sample-Aware* training algorithm for desirable optimality performance with universal feasibility guarantee. Note that in the simulation results on DC-OPF problems in Sec. V, we solve all MILPs of the reformulated calibration magnitude programs (6)-(7) to zero optimality gap. We summarize the result in the following proposition.

Proposition 1. Consider the OPLC, i.e., g_j are all linear, $\forall j = 1, \dots, m$, we can obtain a lower bound on the maximum calibration magnitude in polynomial time. Such a lower bound guarantees the input parameter region \mathcal{D} is preserved.

⁴We remark that the uniform calibration method may introduce the asymmetry on the calibration magnitude as large limit would have large calibration magnitude. An alternative approach is to set the individual calibration rate η_j for each constraint while maintain the supported input region. We refer to Appendix A for a discussion and leave it for future study.

⁵For general OPCC, we may only obtain the *upper bound* on the maximal calibration magnitude if the proposed program is not solved global optimally which can not preserve the input region \mathcal{D} . Such a larger calibration rate could cause some input parameter θ to be infeasible and hence lead the target mapping to learn (from input θ to (sub)optimal solution of OPCC with calibrated constraints) to be illegitimate and not valid within the entire input domain \mathcal{D} .

With the obtained constraints calibration magnitude (or its lower bound), we show how to obtain the DNN model with sufficient size to ensure the universal feasibility over the entire parameter input region despite of the approximation errors in next subsection.

C. Feasibility Guarantee of DNN

1) *DNN Model*: After determining the proper constraints calibrations magnitude, we need train a DNN to learn the input-solution mapping for the problem with calibrated constraints. As discussed in Sec. III, the mapping between the input and the optimal solution of OPCC is continuous if OPCC admits a unique solution for each input $\theta \in \mathcal{D}$ [6], [67]. Existing works [67], [71]–[74] show that the feed-forward neural networks demonstrate universal approximation capability and can approximate real-valued continuous functions arbitrary well for the sufficient large neural network size, indicating that there always exists a DNN size such that universal feasibility can be achieved. Specifically, we employ a DNN model based on a multi-layer feed-forward neural network structure to approximate the input-solution mapping. The DNN model is defined as:

$$\begin{aligned} h_0 &= \theta, \\ h_i &= \sigma(W_i h_{i-1} + b_i), \forall i = 1, \dots, N_{\text{hid}}, \\ \hat{\mathbf{x}} &= \sigma'(W_o h_{N_{\text{hid}}} + b_o), \end{aligned} \tag{8}$$

where θ is the input parameter of the OPCC and forms the input of the DNN. Here we consider a DNN size of N_{hid} hidden layers (depth) and each hidden layer has N_{neu} neurons (width).⁶ h_i is the output the i -th layer, calculated from the i -th layer's weight matrix W_i , bias vector b_i , and the output of the $(i-1)$ -th layer h_{i-1} . $\sigma(x) = \max(x, 0)$ is the applied ReLU activation functions⁷ in the hidden layers and the output layer. Here the $\max(x, 0)$ means taking element-wise max operation over the included vector. $\sigma'(x)$ denotes the two ReLU operations in the output layer such that

$$\begin{aligned} \tilde{h} &= \sigma(W_o h_{N_{\text{hid}}} + b_o - \underline{\mathbf{x}}) + \underline{\mathbf{x}}, \\ \hat{\mathbf{x}} &= -\sigma(\bar{\mathbf{x}} - \tilde{h}) + \bar{\mathbf{x}}. \end{aligned} \tag{9}$$

Here \tilde{h} is the intermediate vector enforcing the lower bound feasibility of predictions. $\hat{\mathbf{x}} = \{\hat{x}_i\}_{i \in \mathcal{P}}$, $\bar{\mathbf{x}}$, $\underline{\mathbf{x}}$ are the predictions, upper bounds, and lower bounds of the variables in \mathcal{P} respectively. We remark that the last two operations in (9) enforces the predicted variables \hat{x}_i to be within its lower bound \underline{x}_i and upper bound \bar{x}_i , and thus, the predicted variables are always feasible.

2) *The Input-Output relations of DNN with ReLU activation*.: To include the neural network equations in the proposed optimization problem, we present the mixed-integer reformulation of the DNNs with ReLUs in the following. Such reformulation is further applied to study the worst-case violation of DNNs. It is known that

⁶The DNNs with different number of neurons can be cast to this structure by setting N_{neu} as the maximum number of neurons among each layer and keep some parameters of the DNN as constant.

⁷The ReLU activation function is widely adopted with the advantage of accelerating the convergence and alleviate the vanishing gradient problem [75]

the maximum operator in ReLU activations in (8) and (9) can be reformulated as a set of mixed-integer linear inequalities. For example, consider the output vector of the k -th hidden layer:

$$h_k = \max(W_k h_{k-1} + b_{k-1}, 0), \forall k = 1, \dots, N_{\text{hid}}$$

For ease of representation, we use \hat{h}_k to denote $W_k h_{k-1} + b_{k-1}$. We adopt the similar formulation as in [14], [15] to reformulate the $\max(\cdot)$ operator:⁸

$$\begin{aligned} h_k^i &\leq \hat{h}_k^i - h_k^{\min, i}(1 - z_k^i), & \forall i = 1, \dots, N_{\text{neu}} \\ h_k^i &\geq \hat{h}_k^i, & \forall i = 1, \dots, N_{\text{neu}} \\ h_k^i &\leq h_k^{\max, i} z_k^i, & \forall i = 1, \dots, N_{\text{neu}} \\ h_k^i &\geq 0, & \forall i = 1, \dots, N_{\text{neu}} \\ z_k &\in \{0, 1\}^{N_{\text{neu}}}. \end{aligned} \tag{10}$$

Here we use the superscript i to denote the i -th element of the vector. z_k are the introduced binary variables. $h_k^{\max, i}$ and $h_k^{\min, i}$ are the upper and lower bounds on the neuron outputs that have to be chosen large/small enough to not be binding. In practice, one can set these bounds to be some large/small numbers. We remark that when the input to the i -th neuron in layer k , $\hat{h}_k^i \leq 0$, the corresponding binary variable z_k^i is 0 such that the last two inequalities in (10) contain it to zero. while the first two are not binding if $\hat{h}_k^i < 0$. Similarly, when $\hat{h}_k^i \geq 0$, the corresponding binary variable z_k^i is 1 such that the first two inequalities in (10) contain it to \hat{h}_k^i while the last two are not binding if $\hat{h}_k^i > 0$.

Typically, the DNN is trained to minimize the average of the specified loss function among the training set by optimizing the the value of W_i and b_i at each layer. In the previous work, the training (test) set is generally obtained by sampling the input data according to some distribution to train (evaluate) the DNN performance [6], [13]. However, the DNN model obtained from such approaches may not achieve good feasibility performance over the entire input domain \mathcal{D} especially considering the worst-case scenarios [14], [45], [46]. In the following, we study the worst-case performance of DNN and determine the sufficient DNN size so that for any possible input from the input region, the resulting DNN solution is guaranteed to be feasible w.r.t. inequality constraints.

3) *Sufficient DNN size in Guaranteeing Universal Feasibility*: We propose the following bi-level program to investigate the learning ability of DNN and determine the sufficient DNN size in ensuring feasibility of the predicted

⁸We remark that there exist other $\max()$ reformulation methods, e.g., MPEC reformulation (which can also be cast as the integer formulation equivalently). In this work, we focus on the mixed-integer linear expression as shown in (10) for an analysis. Such expression shows benefits when designing the framework as discussed in Sec. IV-C4 and Sec. IV-D1

solutions given its structure, considering the worst input:

$$\min_{W_i, b_i} \max_{\boldsymbol{\theta}} \nu^f \quad (11)$$

s.t. (2), (9), (10), $k = 1, \dots, N_{\text{hid}}$, $\boldsymbol{\theta} \in \mathcal{D}$,

$$t_j = \frac{g_j(\boldsymbol{\theta}, \hat{\mathbf{x}}) - \hat{e}_j}{|e_j|}, \forall j = 1, \dots, |\mathcal{E}|, \quad (12)$$

$$\nu^f \geq t_j, \nu^f \leq t_j + M \cdot (1 - b_j), b_j \in \{0, 1\}, \forall j = 0, 1, \dots, |\mathcal{E}|, \quad (13)$$

$$t_0 = 0, \sum_{j=0}^{|\mathcal{E}|} b_j = 1. \quad (14)$$

Constraint (2) represents the set of equality equations. (9) and (10), $k = 1, \dots, N_{\text{hid}}$ represent the correlation between the input $\boldsymbol{\theta}$ of the DNN to its predicted variables $\hat{\mathbf{x}}$ via the formulated DNN constraints. (12) denotes the relative violation on each constraint considering the limits calibration, where $\hat{e}_j = (1_{e_j \geq 0}(1 - \Delta) + 1_{e_j < 0}(1 + \Delta)) \cdot e_j$ denotes the constraint limit after calibration and Δ represents the determined calibration rate via (6)-(7). Here recall that for the class of OPLC, the obtained Δ is no greater than the maximal one⁹ with which the target input parameter region is still guaranteed to be preserved. Consider the inner maximization problem, the objective ν^f hence find the maximum violation among all the constraints consider the worst-case input $\boldsymbol{\theta}$ given the value of DNN parameters $(W_i, b_i, i = 1, \dots, N_{\text{hid}})$. Such maximum violation can be expressed via (13)-(14), in which $b_j, j = 0, \dots, |\mathcal{E}|$ are binary variables that indicate the maximum among t_j (e.g., $b_k = 1$ if t_k is the maximal one) and M can be set as some big number. The optimal value of (11)-(14), denoted as ν^{f*} , represents the maximum relative violation at the inequality constraints, under the worst-case input $\boldsymbol{\theta}$, given the best performance of DNN. Such value presents the feasibility guarantee performance of the DNN. Note that the non-critical constraints are always respected from Definition 1. If $\nu^{f*} \leq \Delta$, meaning the largest violation at the calibrated inequality constraints is no greater than the calibration magnitude. Therefore, the DNN is capable of achieving zero violation at all original inequality constraints for all inputs $\boldsymbol{\theta} \in \mathcal{D}$, and hence, preserving universal feasibility. We remark that solving (11)-(14) can be essentially seen as the training process of the DNN with the calibrated constraints (the iterative approach with gradient decent) such that the maximum violation is minimized from the outer minimization problem over the DNN parameters $(W_i, b_i, i = 1, \dots, N_{\text{hid}})$.

The above program helps to verify whether a certain DNN is capable of achieving universal feasibility within the input parameter region. If $\nu^{f*} > \Delta$, meaning that the test DNN fails to preserve universal feasibility, and we need to enlarge the DNN size, e.g., increase the number of neurons on each layer, such that universal feasibility of DNN solution can be guaranteed. Such DNN size is guaranteed to exist from the universal approximation capability [67], [71]–[74] of DNNs given the condition that the target mapping (from input $\boldsymbol{\theta}$ to (sub)optimal solution of OPCC with calibrated constraints) is continuous and the DNN width N_{neu} is sufficiently large. We highlight the claim of *Universal Approximation* of DNNs in the following proposition.

⁹For OPLC, the obtained Δ is the global maximum or the lower bound of the maximal calibration rate. See Sec. IV-B2 for the discussion.

Proposition 2. [67], [71]–[74] Assume the target function to learn is continuous, there always exists a DNN whose output function can approach the target function arbitrarily well, i.e.,

$$\max_{\theta \in \mathcal{D}} \|h(\theta) - \hat{h}(\theta)\| < \epsilon,$$

hold for any ϵ arbitrarily small (distance from h to \hat{h} can be infinitely small). Here $h(\theta)$ and $\hat{h}(\theta)$ represent the target mapping to be approximated and the DNN function respectively.

Furthermore, given the fixed depth N_{hid} of the DNN, the learning ability of the DNN is increasing monotonically w.r.t. the width of the DNN. That is, consider two DNN width NN_{neu}^1 and NN_{neu}^2 such that $NN_{\text{neu}}^1 > NN_{\text{neu}}^2$, we have

$$\min_{h \in \mathcal{C}^{NN^1}} \max_{\theta \in \mathcal{D}} \|h(\theta) - \hat{h}(\theta)\| \leq \min_{h \in \mathcal{C}^{NN^2}} \max_{\theta \in \mathcal{D}} \|h(\theta) - \hat{h}(\theta)\|,$$

where \mathcal{C}^{NN^1} and \mathcal{C}^{NN^2} denote the class of all functions generated by a N_{hid} depth neural network with width NN_{neu}^1 and NN_{neu}^2 respectively.

Proposition 2 provides as the strong observation and theoretical basis for further designing the iterative approach to determine the sufficient DNN size in guaranteeing universal feasibility.

a) *Iterative Approach for Sufficient DNN Size*: Here (11)–(14) is a non-convex mixed-integer linear bi-level program due to the non-convex equality constraints related to the ReLU activations. Since the inner maximization problem is a mixed-integer nonlinear program, the techniques for convex bi-level programs discussed in Sec. IV-B are not applicable, i.e., replacing the lower-level optimization problem by its KKT conditions. To solve such bi-level optimization problem, we apply the *Danskin’s Theorem* idea to optimize the upper-level variables $(W_i, b_i, i = 1, \dots, N_{\text{hid}})$ by gradient descent. This would simply require to 1) find the maximum of the inner problem, and 2) compute the normal gradient evaluated at this point [76], [77]. We refer interested readers to [78], [79] and Appendix A for the detailed procedures and discussions. After solving the program, we can obtain the optimal value (or the corresponding bound) of (11)–(14) which represents whether a verified DNN size can guarantee universal feasibility. In the following, we propose an iterative approach to determine the sufficient DNN size such that universal feasibility is guaranteed. We start with the initial DNN with depth N_{hid} and width N_{neu} at iteration $t = 0$.

- Step 1. At iteration t , verify the universal feasibility guarantee of DNN with depth N_{hid} and width N_{neu} by solving (11)–(14). If the obtained value $\nu^{f*} \leq \Delta$, stop the iteration.
- Step 2. If $\nu^{f*} > \Delta$, double the DNN width $N_{\text{neu}} \leftarrow 2 \times N_{\text{neu}}$ and proceed to the next iteration $t + 1$. Go to Step 1.

The above approach is expected to determine the sufficient DNN size (width) that is capable of achieving universal feasibility w.r.t. the input domain \mathcal{D} , i.e., $\nu^{f*} - \Delta \leq 0$, if the DNN width is large enough [73]. We use $\mathbf{NN}^{\text{size}}$ to denote the identified sufficient DNN size (width). Note that if the initial tested DNN size guarantees universal

feasibility, we do not need the above doubling approach to further expand the DNN size but keep it as the sufficient one.

We remark that the obtained sufficient DNN size by doubling the DNN width may be substantial, introducing additional training time to train the DNN model and higher computational time when applied to solve OPCC. One can also determine the corresponding minimal sufficient DNN size by a simple and efficient binary search between

- the obtained sufficient DNN size $\mathbf{NN}^{\text{size}}$ and the pre-obtained DNN size $\frac{\mathbf{NN}^{\text{size}}}{2}$ (before doubling the DNN width) which fails to achieve universal feasibility, if the initial tested DNN can not guarantee universal feasibility;
- the initial tested DNN size and some small DNN, e.g., zero width DNN, if the initial tested DNN size is sufficient in guaranteeing universal feasibility.

Such a minimal sufficient DNN size denotes the minimal width required for a given DNN structure with depth N_{hid} to achieve universal feasibility within the entire input domain. We use $\hat{\mathbf{NN}}^{\text{size}}$ to denote the determined minimal sufficient DNN size and propose the following proposition.

Proposition 3. *Consider the DNN width $\hat{\mathbf{NN}}^{\text{size}}$ and assume (11)-(14) is solved global optimally such that $\nu^{f*} - \Delta \leq 0$, any DNN with depth N_{hid} and a smaller width than $\hat{\mathbf{NN}}^{\text{size}}$ can not guarantee universal feasibility for all input $\theta \in \mathcal{D}$. Meanwhile, any DNN with at least $\hat{\mathbf{NN}}^{\text{size}}$ width can always achieve universal feasibility.*

It is worth noticing that the above result is based on the condition that we can obtain the global optimal solution of (11)-(14). However, one should note that the applied procedures based on *Danskin's Theorem* are not guaranteed to provide the global optimal one. In addition, the inner maximization of (11)-(14) is indeed a non-convex mixed-integer nonlinear program due to non-convex equality constraints related to the ReLU activations for general OPCC. The existing solvers, e.g., APOPT, YALMIP, or Gurobi, may not be able to generate the global optimal solution. We refer to Appendix A for a discussion on the relationship between the obtained value and the global optimal one for general OPCC. Despite of the non-global optimality of the solvers/approach, we remark that for the class of OPLC, we can still obtain a useful upper bound for further analysis.

4) *Special Case: OPLC:* We remark that for the class of OPLC, i.e., g_j are all linear, $\forall j = 1, \dots, m$, the inner problem of (11)-(14) is indeed an MILP and we can actually obtain an upper bound on ν^{f*} if program (11)-(14) is not solved to global optimum, meaning that the maximum violation is not beyond such a magnitude. Though such an upper bound might not be tight, it indicates that it is guaranteed to achieve universal feasibility with such a DNN size if it is no greater than Δ . In addition, despite of the difficulty of the mixed-integer non-convex programs that we need to solve repeatedly, we can always obtain a feasible (sub-optimal) solution for further use for both

general OPCC and OPLC.¹⁰ Our simulation results in Sec. V demonstrate such observation. We highlight the result in the following proposition.

Proposition 4. *Consider the OPLC, i.e., g_j are all linear, $\forall j = 1, \dots, m$, and the DNN model defined in (8), we can obtain an upper bound on ν^{f*} in polynomial time. If such a lower bound is no greater than the calibration magnitude Δ , then the determined DNN size is guaranteed to ensure universal feasibility for any input in \mathcal{D} .*

In our case study in Sec. V, we observe that the evaluated initial DNN size can always guarantee universal feasibility with a non-positive worst-case constraints violation. We further conduct simulations with such determined sufficient DNN size $\mathbf{NN}^{\text{size}}$ and leave the analysis of finding the minimal sufficient DNN size (width) $\hat{\mathbf{NN}}^{\text{size}}$ and solving the problem (11)-(14) global optimally for general OPCC for future investigation.

D. Adversary Sample-Aware Algorithm

Note that the corresponding DNN parameters are determined after solving the bi-level optimization problem (11)-(14) to determine the sufficient DNN size. While it is conceivable to use these parameters directly to obtain a complete DNN with good feasibility performance, it may not have good optimality result. We investigate the performances and approximation accuracy of such DNN in the case study in Sec. V-E. To address this issue, we propose a new training algorithm could obtain a DNN model with desirable optimality while guaranteeing universal feasibility within the input domain in this subsection. Overall, we can obtain two DNNs from the framework. Though the first one from determining the sufficient DNN size can guarantee universal feasibility, the other from the proposed training algorithm in this subsection further improves optimality without sacrificing DNN's universal feasibility.

In this subsection, we present *Adversary Sample-Aware*, a new active and adversarial training method to obtain the DNN model with desirable optimality performance while preserving the universal feasibility. It is based on the worst-case inputs identification and attempts to improve the DNN approximation ability around these adversary inputs with violations, i.e., better learning the specific mapping information enclosing some particular input points. The corresponding pseudocode is given in Algorithm 1. The algorithm contains the following two techniques:

Adversary sample identification. The framework sequentially identifies the worst-case input in the entire input \mathcal{D} , at which constraints violations happens given the specification of DNN parameters. This step helps test whether universal feasibility is achieved and find out the potential adversary inputs that cause infeasibility. This step corresponds to line 3-4 in Algorithm 1.

Training based on adversary inputs. We correct the DNN approximation behavior by involving the specific mapping information around the identified adversary samples. In particular, we sequentially include the worst-case inputs identified in the previous step into the training set, anticipating the post-trained DNNs can eliminate violations

¹⁰Such a feasible (sub-optimal) solution can be easily obtained by a heuristic trial of some particular θ , e.g., the worst-case input at the previous round as the initial point and the associate integer values in the constraints, which are fixed given the specification of DNN parameters.

Algorithm 1: Adversary Sample-Aware algorithm

Input: Pre-trained initial neural network \mathcal{NN}_0^0 , training epochs T , number of iterations I , initial training data-set \mathcal{T}^0 , number of auxiliary training samples K , constant a for constructing auxiliary training set

Output: Trained DNN with feasibility guarantee

```

1  $t = 0$ 
2 for  $t < I$  do
3   Find the maximum violation given parameters  $(W^t, b^t)$  of  $\mathcal{NN}_0^t$  by solving:

$$\boldsymbol{\theta}^t = \arg \max_{\boldsymbol{\theta}} \nu^f \quad \text{s.t. (2), (9), (10), } k = 1, \dots, N_{\text{hid}}, \boldsymbol{\theta} \in \mathcal{D}, (12) - (14)$$

4   Save  $\nu^f(\boldsymbol{\theta}^t)$  as the optimal value of the above program with solution  $\boldsymbol{\theta}^t$ .
5   if  $\nu^f(\boldsymbol{\theta}^t) \leq \Delta$  then
6     Break
7   else
8     Construct  $(\boldsymbol{\theta}^{t,i}, \mathbf{x}^{t,i})$  pair set  $S^t$  by uniformly sampling centered around  $\boldsymbol{\theta}^t$  with calibrated OPCC (OPCCc) solutions, for  $i = 0, 1, \dots, K$ :

$$\boldsymbol{\theta}^{t,i} = \boldsymbol{\theta}^t \odot (\mathbf{1} + \boldsymbol{\epsilon}_i) \in \mathcal{D}, \boldsymbol{\epsilon}_i^{(k)} \sim U(-a, a), \mathbf{x}^{t,i} = \text{OPCC}^c(\boldsymbol{\theta}^{t,i})$$

9   Combine  $\mathcal{S}^t$  and  $\mathcal{T}^t$  to get  $\mathcal{T}^{t+1}$ 
10   $j = 0$ 
11  for  $j < T$  do
12    Initial DNN as  $\mathcal{NN}_j^t$  and train on  $\mathcal{T}^{t+1}$  to minimize the loss function (15) by optimizing the DNN parameters;
13    Obtain DNN  $\mathcal{NN}_{j+1}^t$ 
14    if  $\hat{\mathbf{x}}_i^{t,i} \leftarrow \mathcal{NN}_{j+1}^t(\boldsymbol{\theta}^{t,i})$  is feasible w.r.t the original inequality constraints for every  $\boldsymbol{\theta}^{t,i} \in S^t$  then
15      Save  $\mathcal{NN}_{j+1}^t$  as  $\mathcal{NN}_0^{t+1}$ ;
16      Break
17    else if  $j = T - 1$  then
18      Save  $\mathcal{NN}_{j+1}^t$  as  $\mathcal{NN}_0^{t+1}$ 
19     $j = j + 1$ 
20   $t = t + 1$ 

```

*We only include feasible $\boldsymbol{\theta}^{t,i} \in \mathcal{D}$ into S^t . Here $\boldsymbol{\epsilon}_0$ is set to be 0 such that $(\boldsymbol{\theta}^t, \text{OPCC}^c(\boldsymbol{\theta}^t)) \in S^t$ and each element of $\boldsymbol{\epsilon}_i \in \mathcal{R}^M$ is from a uniform distribution $U(-a, a)$ for $i = 1, \dots, K$. \odot denotes the element-wise multiplication operation among two vectors (Hadamard product).

around such inputs by improve its approximation ability around them. In this work, we adopt the supervised learning

approach and design \mathcal{L}^k among the training set consisting of two part:

$$\mathcal{L}^k = w_1 \cdot \frac{1}{n-p} \sum_{i \in \mathcal{P}} (\hat{x}_i - x_i^*)^2 + w_2 \cdot \frac{1}{|\mathcal{E}|} \sum_{j \in \mathcal{E}} \max(g_j([\hat{\mathbf{x}}, \psi_{\theta}(\hat{\mathbf{x}})], \theta), \hat{e}_j), \quad (15)$$

The first part is the mean square error between the predicted variables \hat{x}_i and the reference optimal ones x_i^* . The second part consists of penalty terms related to the inequality constraints violations. w_1 and w_2 are positive weighting factors to balance prediction error and penalty. We use $\psi_{\theta}(\hat{\mathbf{x}})$ to denote the recovered variables via the linear equations (2). We remark that after the constraints calibration, the penalty loss is with respect to the adjusted limits \hat{e}_j discussed in Sec. IV-A. The training processing can be regarded as minimizing the average value of loss function with the given training data by tuning the parameters of the DNN model, including each layer's connection weight matrix and bias vector. This step corresponds to line 5-19 in Algorithm 1. We will discuss the insights and the detailed steps in the following.

The proposed algorithm adopts adversarial learning idea [80], e.g., improving the DNN robustness by providing adversary inputs with violation. Furthermore, we leverage the idea of active learning [81] to improve the training efficiency by sampling around such identified adversary inputs and incorporate the preventive training scheme to enhance the feasibility performance. We remark that the proposed *Adversary Sample-Aware* algorithm is expected to achieve universal feasibility within the entire input domain while preserving desirable optimality performance. The underlining reason lies in that during the adversarial sample identification-training process, both optimality (represented by the prediction error in the first term in (15)) and feasibility (represented by the penalty w.r.t. the constraints violations in the second term in (15)) are considered by training the DNN on such algorithmic designed training set. Therefore, the obtained DNN can improve the feasibility and optimality performance simultaneously by having better approximation accuracy on these samples.

For better representation, we use $\text{OPCC}(\theta)$ and $\text{OPCC}^c(\theta)$ to denote the optimal solutions of the OPCC problem and the OPCC problem with constraints calibrations given the input θ . We remark that with the obtained lower bound on the maximum calibration magnitude Δ , such constraints calibrations only leads to the (sub)-optimal solutions that are interior points within the original feasible region (the inequality constraints are expected to be not binding) while the input parameter region \mathcal{D} in consideration is not reduced.¹¹ Overall, our algorithm, start from round $t = 0$, contains the following steps.

- Step 1. At round t , identify the worst-case input θ^t within the entire input domain \mathcal{D} (line 3-6). If the obtained optimal objective value $\nu^f(\theta^t) \leq \Delta$, stop the iteration.
- Step 2. If $\nu^f(\theta^t) > \Delta$, construct an auxiliary subset S^t containing training pairs $(\theta^{t,i}, \mathbf{x}^{t,i})$ by uniformly sampling centered around θ^t and the associated calibrated OPCC solutions (line 5-8).
- Step 3. Further train the DNN on the new training set \mathcal{T}^{t+1} that combines S^t and the pre-obtained set

¹¹It is expected that a larger calibration magnitude can help to improve the DNN solution feasibility during training. With a smaller calibration rate (lower bound), one may need to increase the DNN model size and the amount of training data/time for better approximation ability to achieve satisfactory feasibility performance.

\mathcal{T}^t (line 9) using back-propagation to minimize the loss function (15) considering constraints calibrations with the chosen training algorithm, e.g., stochastic gradient descent (SGD) with momentum [82] (line 10-13).

- Step 4. Check whether feasibility at the identified adversary sample θ^t at Step 1 (with violation) is restored by the post-trained DNN (line 14-18). If so, proceed to the next round $t + 1$ and go to Step 1.

We expect that after a few training epochs, the post-trained DNN can restore feasibility at the identified adversary sample θ^t and the points around it in \mathcal{S}^t . This is inspired by the observation that after adding the previously identified training pairs \mathcal{S}^t into the training set, the DNN training loss is dominated by the approximation errors and the penalties at the samples in \mathcal{S}^t . Though the training loss may not be optimized to 0, e.g., still has violations w.r.t. the calibrated constraints limits, the DNN solution is expected to satisfy the original inequality constraints after such preventive training procedure. Therefore, the post-trained DNN is capable of preserving feasibility and good accuracy at these input regions. We remark that the algorithm terminates when the maximal relative violation is no greater than the calibration magnitude, i.e., $\nu^{f*} \leq \Delta$ (line 5), such that universal feasibility is guaranteed. Simulation results in Sec. V-E show the effectiveness of the propose algorithm. We provide the following proposition to state the guarantee of the algorithm in ensuring universal feasibility.

Proposition 5. *Consider a DNN with size satisfying the requirement in (11)-(14) to preserve universal feasibility and assume the post-trained \mathcal{NN}_0^{t+1} can maintain feasibility at the constructed neighborhood around θ^i with some small constant a : $\hat{\mathcal{D}}^i = \{\theta | \theta^i \cdot (1-a) \leq \theta \leq \theta^i \cdot (1+a), \theta \in \mathcal{D}\}, \forall i \leq t$ at each iteration t , the proposed Adversary Sample-Aware algorithm is guaranteed to ensure universal feasibility as the number of iterations t tends to infinity.*

Proof idea: Here we consider the post-trained DNN \mathcal{NN}_0^{t+1} can always maintain feasibility at the constructed neighborhoods $\hat{\mathcal{D}}^i, \forall i \leq t$ by training on \mathcal{T}^{t+1} that combines \mathcal{T}^0 and all the auxiliary subset \mathcal{S}^i around the identified adversary input θ^i at each iteration $i \leq t$. Such condition generally requires the DNN to preserve feasibility within some small regions by specially including the input-solution characteristics during training, which may not be hard to satisfy. This can be understood from the observation that the worst-case violation in the smaller inner domain can be reduced significantly by training on the larger outer input domain [14] as the adversary inputs are always element-wise at the boundary of the entire input domain \mathcal{D} , which echoes the our simulation finding in Sec. V. Therefore, the post-trained DNN is expected to perform good feasibility guarantee in each small region $\hat{\mathcal{D}}^t$ after the preventive training procedure on \mathcal{T}^{t+1} , the training set of the entire domain \mathcal{D} . We remark that after gradually including these subsets \mathcal{S}^i into the training set, the loss function is actually determined by the joint loss among all samples in these region. After the training process, the post-obtained DNN is hence expected to maintain feasibility at the points in the training set and the regions around them. Therefore, when the number of iterations t tends to infinity, the union of the feasible regions $\tilde{\mathcal{D}}^{t \rightarrow \infty} = \hat{\mathcal{D}}^1 \cup \hat{\mathcal{D}}^2 \cup \dots \hat{\mathcal{D}}^t$ can cover the entire input domain \mathcal{D} . That is, the post-trained DNN $\mathcal{NN}_0^{t \rightarrow \infty}$ can ensure feasibility for each small region $\hat{\mathcal{D}}^t$ within the input domain \mathcal{D} , and hence universal feasibility is guaranteed.

The above result states that the *Adversary Sample-Aware* algorithm can ensure universal feasibility by pro-

gressively improving the learning ability of DNN around each possible adversary point/region that may cause infeasibility. Therefore, the DNN gradually better learn the global mapping information at each iteration benefit from the ideas of adversarial learning and active learning [80], [81]. Though the results claim the feasibility guarantee as $t \rightarrow \infty$, we remark that in the case study in Sec. V, the proposed *Adversary Sample-Aware* algorithm can achieve universal feasibility with at most 56 iterations, i.e., $\nu^{f*} \leq \Delta$, which indicates the efficiency and usefulness of the proposed training algorithm.

Note that at the *Adversary sample identification* step, the involved program (line 3-4) is a mixed-integer non-convex problem. The existing solvers, e.g., Gurobi, CPLEX, or APOPT, may not be able to generate the global optimal solution due to the high complexity of the non-convex combinatorial problem. In the following, we present that we can still obtain a useful upper bound for the class of OPLC.

1) *Special Case: OPLC*: We remark that for the class of OPLC, i.e., g_j are all linear, $\forall j = 1, \dots, m$, the concerned problem of *Adversary sample identification* is the form of MILP. Though the MILP may not be solved to global optimum, we can still use the obtained *upper bound* to verify the performance of the obtained DNN. If the obtained objective (or its upper bound) is no greater than the calibration magnitude, then universal feasibility of the trained DNN is guaranteed. In addition, despite of the difficulty of the mixed-integer non-convex programs that we need to solve repeatedly, we can always obtain a feasible (sub-optimal) solution for further use for both general OPCC and OPLC.¹² Our simulation results in Sec. V demonstrate such observation. We highlight the result in the following proposition.

Proposition 6. *Consider the OPLC, i.e., g_j are all linear, $\forall j = 1, \dots, m$, and the DNN model defined in (8), we can obtain an upper bound on maximal violation $\nu^f(\theta^t)$ in polynomial time at each iteration t . If such an upper bound is no greater than the calibration magnitude Δ , then the obtained DNN model is guaranteed to ensure universal feasibility for any input in \mathcal{D} .*

Overall, the framework can ensure DNN solution feasibility based on the preventive learning approach and is expected to maintain good DNN optimality performance without sacrificing feasibility guarantee via the proposed *Adversary Sample-Aware* training algorithm. Our simulation results in Sec. V show the effectiveness of the framework.

E. Run-time Complexity of the Framework

To better understand the advantage of the proposed framework for solving OPCC problem, we further analyze its computational complexity as follows.

The computational complexity of the framework consists of two parts. The first is the complexity of using DNN to predict the part solutions in \mathcal{P} , which is $\mathcal{O}(N_{\text{hid}}N_{\text{neu}}^2)$ [5]. Recall that N_{hid} denote the number of hidden layers in DNN (depth), and N_{neu} denotes the number of neurons at each layer (width). In practice, we set N_{neu} to

¹²See the footnote in Sec. IV-C4 for a discussion.

be $\mathcal{O}(N - p)$ and N_{hid} to be 3 to achieve satisfactory optimality and feasibility performance, e.g., see Table II. Therefore, the complexity of using DNN to predict the $N - p$ variables is $\mathcal{O}((N - p)^2)$.

The second part is the complexity of reconstructing the remaining p variables from the predicted part solution in dimension $N - p$ by solving the linear equations in (29). Reconstructing the p variables involves the following two steps: i) calculate the value of $c_i^T \theta$ for each i , which requires $\mathcal{O}(pM)$ operations; ii) solve the linear system with p equations and p variables. It is shown that the complexity is at least $\mathcal{O}(p^2)$ and in general requires $\mathcal{O}(p^3)$ operations [83]. Overall, the computational complexity of the framework is $\mathcal{O}((N - p)^2 + pM + p^3)$.

We then provide the complexity of the traditional method in solving the optimization problems with convex constraints. To the best of our knowledge, the general OPCC does not have complete and universal computational complexity results based on the existing algorithms due to the NP-hardness themselves. To better deliver the results here, we consider the multiparameter quadratic program (mp-QP) formulated as (28)-(31) for an analysis. The mp-QP is wildly adopted with many applications, e.g., DC-OPF problems in power systems and model-predictive control (MPC) problems in general control systems. See Appendix A for the formulation of mp-QP.

Note that the number of decision variables to be optimized is N in the formulated mp-QP. After taking $\mathcal{O}(pM + mM)$ operations to calculate the value of $c_i^T \theta$ for each $i = 1, \dots, p$ and $h_j^T \theta$ for each $j = 1, \dots, m$, the computational complexity of interior-point methods for solving such programs is $\mathcal{O}(N^4)$, measured by the number of elementary operations assuming that it takes a fixed time to execute each operation [66]. Therefore, the traditional method for solve mp-QP has a computational complexity of $\mathcal{O}(N^4 + pM + mM)$.

We remark that the computational complexity of the proposed framework is lower than that of traditional algorithms as $p \leq N$. Our simulation results in Sec. V on DC-OPF problems verify such observation. As seen, the proposed framework provides close-to-optimal solutions (at most 0.43% optimality loss) in a fraction of the time compared with the state-of-the-art solver (up to two order of magnitude speedup).

F. Summary of Results under Different Settings

In this subsection, we briefly summarize the results that can be obtained in polynomial time under the setting of general OPCC and OPLC (g_j are all linear, $\forall j = 1, \dots, m$) if the corresponding program is not solved to global optimum. We discuss the results at **Determine calibration magnitude**, **Determine DNN size for ensuring universal feasibility**, and **Adversary Sample-Aware training algorithm** steps in the proposed framework after i), ii), and iii) in the following respectively.

For general OPCC, we can get i) a upper bound on the maximum calibration magnitude (with the feasible (sub-optimal) solution); ii) a lower bound (with the feasible (sub-optimal) solution) on the worst-case violation given DNN parameters while we may not get the valid and useful result for the bi-level program (11)-(14); iii) a lower bound on the worst-case violation (with the feasible (sub-optimal) solution). In summary, these bounds/results can be loose and may not be utilized with desired performance guarantee.

For OPLC, we can get i) a *valid lower bound* on the maximum calibration magnitude (may or may not not with the feasible solution) that can preserve the input parameter region; ii) a *valid upper bound* on the worst-case violation given DNN parameters (may or may not not with the feasible solution) and the global optimum of the

bi-level MILP program (11)-(14) that can help determine the sufficient DNN size for universal feasibility if it is no greater than the calibration magnitude; 3) a *valid upper bound* on the worst-case violation (may or may not with the feasible solution) that guarantees universal feasibility if it is no greater than the calibration magnitude. In summary, the bounds obtained from the setting of OPLC can still be useful and valid for further analysis.

Furthermore, we state that for each involved program, we can always obtain a feasible (sub-optimal) solution for further use. These results are discussed in the corresponding parts in the paper. Overall, the preventive learning framework provides two DNNs. The first one from characterizing the sufficient DNN size can guarantee universal feasibility while the other from the proposed training algorithm further improves optimality and maintains DNN's universal feasibility simultaneously. Such feasibility guarantee can be verified from the obtained valid bounds specific for OPLC.

V. APPLICATION TO SOLVE DC-OPF PROBLEMS AND NUMERICAL EXPERIMENTS

We apply the framework to develop DeepOPF+ as a feasibility-ensuring scheme for DC-OPF problems in the real world.

A. Problem Formulation

The DC-OPF problem determines optimal generator operations that achieve the least cost while satisfying the physical and operational constraints for each load input $P_D \in \mathcal{R}^{|\mathcal{B}|}$:

$$\min_{P_G, \Phi} \sum_{i \in \mathcal{G}} c_i(P_{Gi}) \quad (16)$$

$$\text{s.t. } P_G^{\min} \leq P_G \leq P_G^{\max}, \quad (17)$$

$$\mathbf{M} \cdot \Phi = P_G - P_D, \quad (18)$$

$$-P_{\text{line}}^{\max} \leq \mathbf{B}_{\text{line}} \cdot \Phi \leq P_{\text{line}}^{\max}, \quad (19)$$

where \mathcal{B} and \mathcal{G} denotes the set of buses and generators respectively. $P_G^{\min} \in \mathcal{R}^{|\mathcal{B}|}$ (resp. P_G^{\max}) and $P_{\text{line}}^{\max} \in \mathcal{R}^{|\mathcal{K}|}$ denote the minimum (resp. maximum) generation output limits of the generators¹³ and the line transmission capacity limits of the branches in the power network, where \mathcal{K} is the set of transmission lines. $\mathbf{M} \in \mathcal{R}^{|\mathcal{B}| \times |\mathcal{B}|}$, $\mathbf{B}_{\text{line}} \in \mathcal{R}^{|\mathcal{K}| \times |\mathcal{B}|}$, and $\Phi \in \mathcal{R}^{|\mathcal{B}|}$ denote the bus admittance matrix, line admittance matrix, and bus phase angles respectively¹⁴. The objective is the total generation cost, i.e., $c_i(\cdot)$ is the cost function of each generator, which is commonly quadratic [84]. Constraints (17)-(19) enforce nodal power balance equations, the limits on the active power generation P_G and line transmission capacity. Note that the slack bus voltage phase angle ϕ^{slack} is fixed to be zero. In general, the DC-OPF problem is a quadratic programming and admits a unique optimal solution w.r.t. each load input P_D .

¹³ $P_{Gi} = P_{Gi}^{\min} = P_{Gi}^{\max} = 0, \forall i \notin \mathcal{G}$, and $P_{Di} = 0, \forall i \notin \mathcal{A}$, where \mathcal{A} denotes the set of load buses.

¹⁴ Here we only consider the branches where they could reach the limits.

1) *Proposed DeepOPF+*: We design the DeepOPF+ for solving DC-OPF problem by adopting the predict-and-reconstruct framework [4]. Specifically, it leverages that the admittance matrix (after removing the entries corresponding to the slack bus) $\tilde{\mathbf{M}}$ is of full rank $B - 1$, where $B = |\mathcal{B}|$ and is the size of the set of buses. Thus, given each P_D , once the non-slack generations $\{P_{Gi}\}_{i \in \mathcal{G} \setminus n_0}$ (n_0 denotes the slack bus index) are determined, the slack generation and the bus phase angles of all buses can be uniquely reconstructed:

$$\begin{aligned} P_G^{\text{slack}} &= \sum_{i \in \mathcal{B}} P_{Di} - \sum_{i \in \mathcal{B} \setminus n_0} P_{Gi}, \\ \tilde{\Theta} &= \tilde{\mathbf{M}}^{-1} (\tilde{P}_G - \tilde{P}_D), \end{aligned} \quad (20)$$

where n_0 and P_G^{slack} denote the slack bus index and slack bus generation respectively. \tilde{P}_G and \tilde{P}_D are the $(B - 1)$ -dimensional generation and load vectors for all buses except the slack bus. Consequently, the line flow capacity constraints in (18) can be reformulated as

$$-P_{\text{line}}^{\max} \leq \tilde{\mathbf{B}}_{\text{line}} \tilde{\mathbf{M}}^{-1} (\tilde{P}_G - \tilde{P}_D) \leq P_{\text{line}}^{\max}, \quad (21)$$

where $\tilde{\mathbf{B}}_{\text{line}}$ is the line admittance matrix after removing the column of slack bus¹⁵. Therefore, we can solve DC-OPF problem by employing DNNs to depict the mapping between P_D and P_G . We further note that any feasible active power generation P_{Gi} that satisfies (17) can be written as

$$P_{Gi} = P_{Gi}^{\min} + \alpha_i \cdot (P_{Gi}^{\max} - P_{Gi}^{\min}), \quad \alpha_i \in [0, 1], i \in \mathcal{G}. \quad (22)$$

Similar to [4], instead of predicting P_G , we use DNNs to generate the corresponding scaling factors and reconstruct the P_G and remaining variables in implementation. Here we apply the Sigmoid function $\sigma'(x) = \frac{1}{1+e^{-x}}$ at the output layer of DNNs to predict the (0,1) scaling factors such that the feasibility of predicted $P_{Gi}, i \in \mathcal{G}$ can be always guaranteed. The Sigmoid functions at the output layer present the same effect of the last two clipped ReLU operations in (9) to ensure feasibility of the predicted variables.

When adopting preventive learning framework for solving DC-OPF problems, we first remove the non-critical inequality constraints for DC-OPF problem as discussed in Appendix A. After that, we determine the inequality constraints calibration magnitude as discussed in Sec. IV-B. As shown in Sec. IV-C and Sec. IV-D, we further derive the DNN model with sufficient size via solving the bi-level optimization problem, and apply the *Adversary Sample-Aware* algorithm to ensure the universal feasibility of its generated solution given the input region without losing optimality. We refer interested readers to Appendix A for a detailed discussion on these steps and provide the following corollary highlighting the feasibility guarantee and the computational efficiency of the obtained DNN.

Corollary 1. *For the studied DC-OPF problem and applied DNN model defined in (8), assume*

- *the obtained maximum calibration rate (or its lower bound) Δ is non-zero;*
- *the determined DNN is sufficient in ensuring universal feasibility (the optimal value (or the upper bound) of (11)-(14) $\nu^{f*} \leq \Delta$);*

¹⁵The matrix $\tilde{\mathbf{B}}_{\text{line}} \tilde{\mathbf{M}}^{-1}$ is well-known as “Power Transfer Distribution Factors” (PTDF) matrix [85].

TABLE II
PARAMETERS FOR TEST CASES.

Case	$ \mathcal{B} $	$ \mathcal{G} $	$ \mathcal{A} $	$ \mathcal{K} $	N_{hid}	Neurons per hidden layer
Case30	30	6	20	41	3	32/16/8
Case118	118	19	99	186	3	128/64/32
Case300	300	69	199	411	3	256/128/64

* \mathcal{A} and \mathcal{K} denote the set of load bus and the set of branches respectively.

* The number of load buses is calculated based on the default load on each bus. A bus is considered a load bus if its default active power consumption is non-zero.

- the maximum relative violation (or its upper bound) among the calibrated constraints of the trained DNN from the Adversary Sample-Aware algorithm is no greater than Δ ;

the obtained DNN guarantees universal feasibility for any input in \mathcal{D} .

Furthermore, the proposed DNN based framework DeepOPF+ has a smaller computational complexity of $\mathcal{O}(B^2)$ compared with that of traditional method $\mathcal{O}(B^4)$, where B is the number of buses.

In the following subsections, we further apply the steps in the proposed DeepOPF+ framework to the DC-OPF problems.

B. Experiment Setup

The experiments are conducted in CentOS 7.6 on the quad-core (i7-3770@3.40G Hz) CPU workstation with 16GB RAM. We evaluate DeepOPF+ on three representative test power networks: IEEE 30-, 118-, and 300-bus test cases [86].¹⁶ For each test case, the amount of training data and test data are 50,000 and 10,000. The load data is sampled within [100%, 130%] of the default load on each load bus uniformly at random, which covers both light-load and heavy-load regimes such that some transmission lines and slack generation reach the allowed operational limits. Note that the existing DNN-based approaches may not be able to provide feasible solution especially under the heavy-load regimes. According to the sizes of the power network, we design DNNs with different neurons on each hidden layer. The parameters are given in Table II. We train the DNNs on the Pytorch platform. The number of training epochs is 200. Based on empirical experience, we set the weighting factors $w_1 = 1$ and $w_2 = 1$. We evaluate the obtained DNNs from different training approaches considering the following criteria:

- Feasibility: What is percentage of the feasible solutions provided by DNN on the test set?
- Universal Feasibility: Whether the obtained DNN can guarantee universal feasibility within the entire load input domain?

¹⁶As IEEE 118-bus and 300-bus test cases provided by MATPOWER [87] do not specify the line capacities, we use IEEE 118-bus test case and the line capacity setting for IEEE 300-bus test case with the same branch provided by Power Grid Lib [88] (version 19.05).

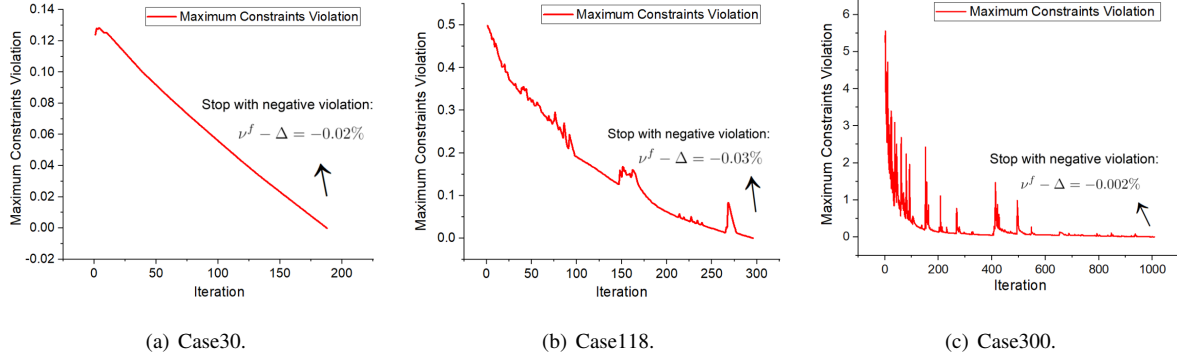


Fig. 2. Maximum relative constraints violation compared with calibration magnitude ($\nu^f - \Delta$) at each iteration for IEEE Case30, Case118, and Case300 test case.

TABLE III
MAXIMUM CALIBRATION RATE ON THE CRITICAL CONSTRAINTS FOR THREE TEST CASES.

Variants	IEEE Case30	IEEE Case118	IEEE Case300
Maximum calibration rate	7.0%	16.7%	21.6%

- Prediction error: What is the difference between the optimal solution and the DNN predicted solution?
- Optimality loss: what is the difference between the cost at the optimal solution and the cost at the solution predicted by DNN?
- Speedup: How fast can the DNN achieve in obtaining the final feasible solution?

C. Critical Constraint Calibration and Universal Feasibility

We will apply the framework DeepOPF+ to solve the DC-OPF problems with the three steps discussed in Sec. IV-B to Sec. IV-D. We first summarize the maximum calibration rate for the three test cases in Table III, showing that the critical inequality constraints can be calibrated by at most 7.0%, 16.7%, and 21.6% for IEEE 30-, 118-, and 300-bus test cases respectively by solving the programs (6)-(7) for each test case. Note that as DC-OPF problem is a convex problem with linear constraints, the program (6)-(7) involved in this step can be reformulated as MILP as discussed in Sec. IV-B2. In this experiment, we remark that we solve these MILPs to zero optimality gap. Therefore, the obtained calibration rate is tight and global optimal. We also verify the feasibility guarantee performance of designed DNNs and show the change of the difference between maximum relative constraints violation and calibration magnitude during solving process in Fig. 2. From Fig. 2, we observe that for all three test cases, the proposed approach succeeds in reaching a relative constraints violation no larger than the corresponding calibration magnitude Δ , i.e., $\nu^f \leq \Delta$, indicating that the DNNs in Table II have enough size to guarantee feasibility within the given load input domain.

TABLE IV
PERFORMANCE EVALUATION OF DNN-BASED APPROACH WITH DIFFERENT CONSTRAINTS CALIBRATION UNDER TYPICAL TRAINING MANNER.

Case	Limit calibration (%)	Feasibility rate (%)	Feasibility rate without calibration (%)	Average cost (\$/hr)			Average running time (ms)		Average speedup
				DeepOPF-Cal*	Ref.	Loss(%)	DeepOPF-Cal	Ref.	
Case30	1.0	98.52	97.65	675.4		0.03	0.51		×85
	3.0	99.73		675.4	675.2	0.03	0.50	43	×86
	5.0	99.99		675.4		0.03	0.50		×86
	7.0	100		675.5		0.04	0.50		×86
Case118	1.0	80.87	54.34	111377.8		0.19	1.27		×164
	3.0	98.60		111472.8	111165.3	0.28	0.71	123	×185
	5.0	99.94		111606.4		0.40	0.58		×213
	7.0	100		111724.9		0.50	0.58		×214
Case300	1.0	94.06	87.73	851247.5		0.04	1.34		×127
	3.0	98.61		851401.3	850882.6	0.06	0.79	84	×134
	5.0	99.73		851695.8		0.10	0.65		×136
	7.0	100		852099.6		0.14	0.60		×140

* DeepOPF-Cal stands for the adopted DeepOPF approach with critical constraints calibration.

TABLE V
PERFORMANCE COMPARISONS OF DEEPOPF+ AND EXISTING DNN-BASED APPROACHES ON TEST CASES.

Variants	Universal Feasibility	Case30			Case118			Case300		
		Prediction error (%)	Optimality loss (%)	Speedup	Prediction error (%)	Optimality loss (%)	Speedup	Prediction error (%)	Optimality loss (%)	Speedup
DeepOPF-Cal	✗	3.4	0.04	86	9.9	0.50	214	2.9	0.14	140
DNN-FG	✓	4.5	0.08	86	39.0	2.42	220	14.6	0.98	138
DeepOPF+	✓	3.5	0.03	87	9.3	0.43	220	0.98	0.07	139

D. Effectiveness of Inequality Constraint Calibration

We first evaluate the effectiveness of constraints calibration on ensuring the feasibility performance on the test set. Specifically, we adopt the DeepOPF approach in [4] (named DeepOPF-Cal) and compare the performance of its variants that are with different calibration rate on the critical constraints. According to the maximum constraints calibration results shown in Table III, the test calibration rates are set as 1.0%, 3.0%, 5.0%, and 7.0% in (5), respectively, which are all no greater than the maximum calibration rate shown in Table III. The DC-OPF problem solution provided by Pypower [89] is regarded as ground truth. For each power network, we train a DNN on the uniformly sampled training set derived in Sec. V-B with loss function (15) to approximate its load-generation mapping. The DNN inputs the load profile and outputs the generation prediction.

For the DNNs from such typical training approach, we observe infeasibility without any calibrations, and feasibility improvement is up to 45.66% on the test set with the preventive calibrations (from 54.34% to 100%).¹⁷ Also, the differences between the average cost of the DNN solutions and that of the reference ones are minor (at

¹⁷If the DNN generates infeasible solutions, we apply an efficient ℓ_1 -projection post-processing procedure to ensure the feasibility of the final solution [5], which is essentially an LP. The average running time includes the post-processing time if DNN obtains infeasible solutions.

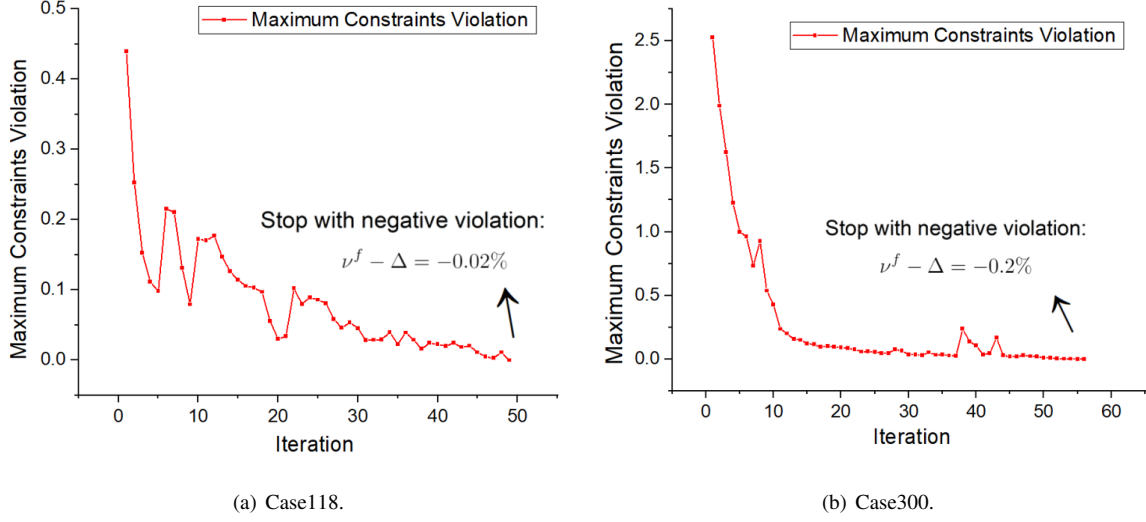


Fig. 3. Performance of *Adversary Sample-Aware* algorithm for IEEE Case118 and IEEE Case300.

most 0.50%). The DNNs speed up the computational time by two orders of magnitude on the test set.¹⁸ Note that the existing DNN-based schemes may not achieve high speedups due to the expensive post-processing procedure to recover the feasibility of infeasible DNN solutions. Moreover, we observe that larger calibration rates contribute to higher feasibility rates but lead to larger optimality losses.¹⁹ Our results demonstrate the effectiveness of critical constraints calibrations and show that all three test cases achieve 100% feasibility with a 7.0% calibration rate on the test set. However, we remark that they cannot guarantee the universal feasibility on the entire input region as their performances under adversary load inputs could be discouraging, as shown in the next subsection.

E. Performance Evaluation of DeepOPF+

We further evaluate the performance of the proposed DeepOPF+. Specifically, we compare the following three DNN-based approaches and show the results in Table V:

- DeepOPF-Cal: the adopted DeepOPF approach [4] with 7.0% calibration rate.
- DNN-FG: the proposed approach (11)-(14) to determine the sufficient DNN size in guaranteeing universal feasibility considering DNN violation minimization.
- DeepOPF+: the proposed DeepOPF+ approach using the *Adversary Sample-Aware* training algorithm. Specifically, the initial model is chosen as the DNN model with 7.0% calibration rate. Maximum training epochs $T = 200$. Initial training data set \mathcal{T}^0 is the same as the one obtained in Sec. V-B, the auxiliary set \mathcal{S}^t size $K = 100$, and the sampling rate $a = 0.01$ around the adversary input P_D^t .

¹⁸Note that Case118 takes a longer computational time to obtain the optimal solution with the conventional solver compared to Case300. This observation comes from the observation that Case118 requires more iteration steps to converge (on average 25 times) than Case300 (on average 11 times), while the average running time per iteration of Case118 (4.7 ms) is less than that of Case300 (7.5 ms).

¹⁹As we employ DNN to approximate the load-solution mapping of calibrated OPF problems, the optimality loss may increase when calibration magnitude is larger, i.e., the sample ground truth deviates more from the optimal solution.

TABLE VI
SPEEDUP PERFORMANCE EVALUATION OF DEEPOPF+ IN THE LIGHT-LOAD AND HEAVY-LOAD REGIMES.

Case	Scheme	Average Speedups		Feasibility rate (%)	
		light-load regime	heavy-load regime	light-load regime	heavy-load regime
Case30	DeepOPF	$\times 87$	$\times 90$	100	92.22
	DeepOPF+	$\times 87$	$\times 93$	100	100
Case118	DeepOPF	$\times 174$	$\times 118$	80.21	53.78
	DeepOPF+	$\times 202$	$\times 228$	100	100
Case300	DeepOPF	$\times 124$	$\times 114$	94.01	82.05
	DeepOPF+	$\times 130$	$\times 138$	100	100

* The average reference DC-OPF time under heavy-load regime is larger than that under light-load regime.

Therefore, DeepOPF+ has a larger speedup under the heavy-load regime compared with the light-load one.

We have following observations from Table V. For DeepOPF-Cal, though it performs well on the test set, it fails to provide universal feasibility in satisfying the operational constraints under worst-case input, i.e., up to 0.71%, 43.96%, and 252.88% violation for Case30, Case118, and Case300, respectively. Such adversary inputs are always element-wise at the boundary of \mathcal{D} , which can be rarely spotted by the applied uniform sampling strategy. As compared with it, both DNN-FG and DeepOPF+ can obtain universal feasibility.

For DNN-FG, though desirable universal feasibility is maintained, its optimality and prediction accuracy performances are substandard, due to only focusing on diminishing violations when optimizing the DNN parameters via (11)-(14). We remark that the performance of DNN-FG is closely related to the initialization of the DNNs. In this experiment, we initialize with the pre-trained DNNs in [13]. Here DNN-FG achieves universal violation within the entire load domain after 187, 295, and 1008 iterations for IEEE Case30, Case118, and Case300, respectively. We refer to Fig. 2 for the relative violation ($\nu^f - \Delta$) for each test case at each iteration for illustration.

For DeepOPF+, we train the DNN at 7.0% calibration rate on set \mathcal{T}^{t+1} at each round. We observe that the post-trained DNN \mathcal{NN}_0^{t+1} can always restore feasibility at the adversary input P_D^t after a few training epochs (maximum 130 epochs while 24 epochs on average for Case300) and benefit from including the adversary load samples in training for smaller worst-case violations.²⁰ We note that the DNN model DeepOPF+ obtained from the *Adversary Sample-Aware* algorithm can preserve desirable accuracy and optimality performance (0.03% loss for Case30, 0.43% loss for Case118 and 0.07% for Case300) while maintaining universal feasibility within the entire load domain. This observation indicates the effectiveness of the *Adversary Sample-Aware* algorithm. We refer to Fig. 3 for the relative violation ($\nu^f - \Delta$) on Case118 and Case300-bus at each iteration for illustration. For Case30, the *Adversary Sample-Aware* algorithm helps achieve universal feasibility just after one iteration (from 0.71% to -0.62%).

²⁰For DeepOPF-Cal, its training loss converges after 200 training epochs and hardly decreases if we keep increasing the number of training epochs.

1) *Performance under Light-load and Heavy-load Settings:* We further test DeepOPF+ under both light-load and heavy-load settings and compare its performance with the existing DNN based scheme DeepOPF [4] without constraints calibrations. The results are reported in Table VI. For the light-load setting, the load variation region is set within [100%, 115%] of the default load. Under such a setting, we observe that only a small portion of test instances constraints are binding in the test data set, e.g., 6.46% for Case300. Under the heavy-load congested setting, the load variation region is set within [115%, 130%] of the default load. Under the setting, the systems constraints are highly binding. e.g., 100% test instances in the test set have binding inequality constraints for Case300. We remark that though the existing DNN scheme DeepOPF may work well in the light-load setting in which the system constraints are not highly binding, its feasibility and speedup performance under the heavy-load regime could be discouraging due to the inherent DNN prediction errors. We observe that DeepOPF+ improves over existing DNN-based schemes in that it achieves consistent speedups in both light-load and heavy-load regimes. As mentioned before, existing DNN-based schemes may need a highly computational complexity post-processing procedure to ensure the feasibility when infeasible DNN solution is observed especially in heavy-load regime, which is not necessary in the proposed DeepOPF+.

In summary, simulation results on Table V demonstrate the improvement of the proposed DeepOPF+ on ensuring universal feasibility over the existing DNN-based approach while achieving desirable optimality and speedup performance.

VI. CONCLUDING REMARKS

In this paper, we propose a preventive learning framework for solving OPCC with solution feasibility guarantee. The idea is to systematically calibrate inequality constraints used in DNN training, thereby anticipating prediction errors and ensuring the resulting solutions remain feasible. The framework includes (i) deriving the maximum calibration magnitude to preserve the supported input region, (ii) determining the sufficient DNN size need for achieving universal feasibility, and (iii) a new *Adversary Sample-Aware* training algorithm to improve the DNN's optimality performance while preserving the constraint feasibility. Overall, the preventive learning framework provides two DNNs. The first one from determining the sufficient DNN size can guarantee universal feasibility while the other from the proposed training algorithm further improves optimality and maintains DNN's universal feasibility simultaneously. We apply the preventive learning framework to develop DeepOPF+ for solving the essential DC-OPF problem in grid operation. Simulation results over IEEE test cases show that DeepOPF+ improves over existing DNN-based schemes in ensuring feasibility and attaining desirable speedup performance in the heavy-load regimes. Moreover, it achieves at most <0.5% optimality loss and up to two orders of magnitude computational speedup, as compared to a state-of-the-art numerical solver.

We note that, despite of the potential of the framework, there are several limitations. First, we evaluate the constraints calibration and performance of DNNs via the proposed programs (6)-(7) and (11)-(14), which are non-convex problems. The current solvers, e.g., Gurobi, CPLEX, or APOPT, may not provide the global optimal solutions and the valid bounds for general OPCC. Second, the proposed framework only focuses on the optimization

problem with convex constraints; extending the framework to general non-convex constrained problems would be an interesting future direction.

REFERENCES

- [1] K. Hornik, M. Stinchcombe, and H. White, "Multilayer feedforward networks are universal approximators," *Neural networks*, vol. 2, no. 5, pp. 359–366, 1989.
- [2] M. Leshno, V. Y. Lin, A. Pinkus, and S. Schocken, "Multilayer feedforward networks with a nonpolynomial activation function can approximate any function," *Neural networks*, vol. 6, no. 6, pp. 861–867, 1993.
- [3] B. Hanin, "Universal function approximation by deep neural nets with bounded width and relu activations," *Mathematics*, vol. 7, no. 10, p. 992, 2019.
- [4] X. Pan, T. Zhao, and M. Chen, "Deepopf: Deep neural network for DC optimal power flow," in *2019 IEEE International Conference on Communications, Control, and Computing Technologies for Smart Grids (SmartGridComm)*. IEEE, 2019, pp. 1–6.
- [5] X. Pan, T. Zhao, M. Chen, and S. Zhang, "Deepopf: A deep neural network approach for security-constrained DC optimal power flow," *IEEE Transactions on Power Systems*, vol. 36, no. 3, pp. 1725–1735, 2020.
- [6] X. Pan, M. Chen, T. Zhao, and S. H. Low, "DeepOPF: A Feasibility-Optimized Deep Neural Network Approach for AC Optimal Power Flow Problems," *arXiv preprint arXiv:2007.01002*, 2020.
- [7] P. L. Donti, D. Rolnick, and J. Z. Kolter, "DC3: A learning method for optimization with hard constraints," *arXiv preprint arXiv:2104.12225*, 2021.
- [8] M. Chatzos, F. Fioretto, T. W. Mak, and P. Van Hentenryck, "High-fidelity machine learning approximations of large-scale optimal power flow," *arXiv preprint arXiv:2006.16356*, 2020.
- [9] X. Lei, Z. Yang, J. Yu, J. Zhao, Q. Gao, and H. Yu, "Data-driven optimal power flow: A physics-informed machine learning approach," *IEEE Transactions on Power Systems*, vol. 36, no. 1, pp. 346–354, 2020.
- [10] W. Huang, X. Pan, M. Chen, and S. H. Low, "DeepOPF-V: Solving AC-OPF Problems Efficiently," *accepted for IEEE Trans. Power Syst.*, 2021.
- [11] H. Sun, X. Chen, Q. Shi, M. Hong, X. Fu, and N. D. Sidiropoulos, "Learning to optimize: Training deep neural networks for interference management," *IEEE Transactions on Signal Processing*, vol. 66, no. 20, pp. 5438–5453, 2018.
- [12] W. Xia, G. Zheng, Y. Zhu, J. Zhang, J. Wang, and A. P. Petropulu, "A deep learning framework for optimization of miso downlink beamforming," *IEEE Transactions on Communications*, vol. 68, no. 3, pp. 1866–1880, 2019.
- [13] T. Zhao, X. Pan, M. Chen, A. Venzke, and S. H. Low, "DeepOPF+: A Deep Neural Network Approach for DC Optimal Power Flow for Ensuring Feasibility," *arXiv preprint arXiv:2009.03147*, 2020.
- [14] A. Venzke, G. Qu, S. Low, and S. Chatzivasileiadis, "Learning optimal power flow: Worst-case guarantees for neural networks," in *2020 IEEE International Conference on Communications, Control, and Computing Technologies for Smart Grids (SmartGridComm)*. IEEE, 2020, pp. 1–7.
- [15] V. Tjeng, K. Y. Xiao, and R. Tedrake, "Evaluating robustness of neural networks with mixed integer programming," in *International Conference on Learning Representations*, 2018.
- [16] F. Li and Y. Du, "From alphago to power system ai: What engineers can learn from solving the most complex board game," *IEEE Power and Energy Magazine*, vol. 16, no. 2, pp. 76–84, 2018.
- [17] L. A. Wehenkel, *Automatic learning techniques in power systems*. Springer Science & Business Media, 2012.
- [18] F. Hasan, A. Kargarian, and A. Mohammadi, "A survey on applications of machine learning for optimal power flow," in *2020 IEEE Texas Power and Energy Conference (TPEC)*. IEEE, 2020, pp. 1–6.
- [19] V. J. Gutierrez-Martinez, C. A. Cañizares, C. R. Fuerte-Esquivel, A. Pizano-Martinez, and X. Gu, "Neural-network security-boundary constrained optimal power flow," *IEEE Transactions on Power Systems*, vol. 26, no. 1, pp. 63–72, 2010.
- [20] A. Vaccaro and C. A. Cañizares, "A knowledge-based framework for power flow and optimal power flow analyses," *IEEE Transactions on Smart Grid*, vol. 9, no. 1, pp. 230–239, 2016.
- [21] L. Halilbašić, F. Thams, A. Venzke, S. Chatzivasileiadis, and P. Pinson, "Data-driven security-constrained AC-OPF for operations and markets," in *2018 Power Systems Computation Conference (PSCC)*. IEEE, 2018, pp. 1–7.
- [22] D. Biagioni, P. Graf, X. Zhang, A. S. Zamzam, K. Baker, and J. King, "Learning-accelerated ADMM for distributed DC optimal power flow," *IEEE Control Systems Letters*, 2020.
- [23] S. Pineda, J. M. Morales, and A. Jiménez-Cordero, "Data-driven screening of network constraints for unit commitment," *IEEE Transactions on Power Systems*, vol. 35, no. 5, pp. 3695–3705, 2020.

[24] M. Jamei, L. Mones, A. Robson, L. White, J. Requeima, and C. Ududec, “Meta-optimization of optimal power flow,” *ICML Workshop, Climate Change: How Can AI Help*, 2019.

[25] D. Deka and S. Misra, “Learning for DC-OPF: Classifying active sets using neural nets,” in *2019 IEEE Milan PowerTech*. IEEE, 2019, pp. 1–6.

[26] S. Karagiannopoulos, P. Aristidou, and G. Hug, “Data-driven local control design for active distribution grids using off-line optimal power flow and machine learning techniques,” *IEEE Transactions on Smart Grid*, vol. 10, no. 6, pp. 6461–6471, 2019.

[27] K. Baker and A. Bernstein, “Joint chance constraints in AC optimal power flow: Improving bounds through learning,” *IEEE Transactions on Smart Grid*, vol. 10, no. 6, pp. 6376–6385, 2019.

[28] Y. Ng, S. Misra, L. A. Roald, and S. Backhaus, “Statistical learning for DC optimal power flow,” in *2018 Power Systems Computation Conference (PSCC)*. IEEE, 2018, pp. 1–7.

[29] S. Misra, L. Roald, and Y. Ng, “Learning for Constrained Optimization: Identifying Optimal Active Constraint Sets,” *arXiv preprint arXiv:1802.09639*, 2018.

[30] Q. Zhai, X. Guan, J. Cheng, and H. Wu, “Fast identification of inactive security constraints in SCUC problems,” *IEEE Transactions on Power Systems*, vol. 25, no. 4, pp. 1946–1954, 2010.

[31] L. A. Roald and D. K. Molzahn, “Implied constraint satisfaction in power system optimization: the impacts of load variations,” in *2019 57th Annual Allerton Conference on Communication, Control, and Computing (Allerton)*. IEEE, 2019, pp. 308–315.

[32] L. Duchesne, E. Karangelos, and L. Wehenkel, “Recent Developments in Machine Learning for Energy Systems Reliability Management,” *Proceedings of the IEEE*, vol. 108, no. 9, pp. 1656–1676, 2020.

[33] Y. Chen and B. Zhang, “Learning to solve network flow problems via neural decoding,” *arXiv preprint arXiv:2002.04091*, 2020.

[34] K. Baker, “Learning warm-start points for AC optimal power flow,” in *2019 IEEE 29th International Workshop on Machine Learning for Signal Processing (MLSP)*. IEEE, 2019, pp. 1–6.

[35] W. Dong, Z. Xie, G. Kestor, and D. Li, “Smart-pgsm: using neural network to accelerate AC-OPF power grid simulation,” in *SC20: International Conference for High Performance Computing, Networking, Storage and Analysis*. IEEE, 2020, pp. 1–15.

[36] M.-F. Balcan, T. Dick, T. Sandholm, and E. Vitercik, “Learning to branch,” in *International conference on machine learning*. PMLR, 2018, pp. 344–353.

[37] H. He, H. Daume III, and J. M. Eisner, “Learning to search in branch and bound algorithms,” *Advances in neural information processing systems*, vol. 27, pp. 3293–3301, 2014.

[38] N. Guha, Z. Wang, M. Wytock, and A. Majumdar, “Machine learning for AC optimal power flow,” *arXiv preprint arXiv:1910.08842*, 2019.

[39] A. S. Zamzam and K. Baker, “Learning optimal solutions for extremely fast AC optimal power flow,” in *2020 IEEE International Conference on Communications, Control, and Computing Technologies for Smart Grids (SmartGridComm)*. IEEE, 2020, pp. 1–6.

[40] F. Fioretto, T. W. Mak, and P. Van Hentenryck, “Predicting AC optimal power flows: Combining deep learning and lagrangian dual methods,” in *Proceedings of the AAAI Conference on Artificial Intelligence*, vol. 34, no. 01, 2020, pp. 630–637.

[41] R. Dobbé, O. Sondermeijer, D. Fridovich-Keil, D. Arnold, D. Callaway, and C. Tomlin, “Toward distributed energy services: Decentralizing optimal power flow with machine learning,” *IEEE Transactions on Smart Grid*, vol. 11, no. 2, pp. 1296–1306, 2019.

[42] E. R. Sanseverino, M. Di Silvestre, L. Mineo, S. Favuzza, N. Nguyen, and Q. Tran, “A multi-agent system reinforcement learning based optimal power flow for islanded microgrids,” in *2016 IEEE 16th International Conference on Environment and Electrical Engineering (EEEIC)*. IEEE, 2016, pp. 1–6.

[43] K. Li and J. Malik, “Learning to optimize,” *arXiv preprint arXiv:1606.01885*, 2016.

[44] Y. Chen, M. W. Hoffman, S. G. Colmenarejo, M. Denil, T. P. Lillicrap, M. Botvinick, and N. Freitas, “Learning to learn without gradient descent by gradient descent,” in *International Conference on Machine Learning*. PMLR, 2017, pp. 748–756.

[45] R. Nellikkath and S. Chatzivasileiadis, “Physics-informed neural networks for minimising worst-case violations in DC optimal power flow,” *arXiv preprint arXiv:2107.00465*, 2021.

[46] —, “Physics-informed neural networks for ac optimal power flow,” *arXiv preprint arXiv:2110.02672*, 2021.

[47] L. Zhang, Y. Chen, and B. Zhang, “A convex neural network solver for DCOPF with generalization guarantees,” *arXiv preprint arXiv:2009.09109*, 2020.

[48] P.-W. Wang, P. Dotti, B. Wilder, and Z. Kolter, “Satnet: Bridging deep learning and logical reasoning using a differentiable satisfiability solver,” in *International Conference on Machine Learning*. PMLR, 2019, pp. 6545–6554.

[49] R. T. Chen, Y. Rubanova, J. Bettencourt, and D. Duvenaud, “Neural ordinary differential equations,” *arXiv preprint arXiv:1806.07366*, 2018.

[50] C. K. Ling, F. Fang, and J. Z. Kolter, “What game are we playing? end-to-end learning in normal and extensive form games,” *arXiv preprint arXiv:1805.02777*, 2018.

[51] F. de Avila Belbute-Peres, K. Smith, K. Allen, J. Tenenbaum, and J. Z. Kolter, “End-to-end differentiable physics for learning and control,” *Advances in neural information processing systems*, vol. 31, pp. 7178–7189, 2018.

[52] S. Bai, J. Z. Kolter, and V. Koltun, “Deep equilibrium models,” *arXiv preprint arXiv:1909.01377*, 2019.

[53] P. L. Donti, B. Amos, and J. Z. Kolter, “Task-based end-to-end model learning in stochastic optimization,” *arXiv preprint arXiv:1703.04529*, 2017.

[54] J. Djolonga and A. Krause, “Differentiable learning of submodular models,” *Advances in Neural Information Processing Systems*, vol. 30, pp. 1013–1023, 2017.

[55] S. Tschiatschek, A. Sahin, and A. Krause, “Differentiable submodular maximization,” *arXiv preprint arXiv:1803.01785*, 2018.

[56] B. Wilder, B. Dilkina, and M. Tambe, “Melding the data-decisions pipeline: Decision-focused learning for combinatorial optimization,” in *Proceedings of the AAAI Conference on Artificial Intelligence*, vol. 33, no. 01, 2019, pp. 1658–1665.

[57] S. Gould, R. Hartley, and D. Campbell, “Deep declarative networks: A new hope,” *arXiv preprint arXiv:1909.04866*, 2019.

[58] B. Amos and J. Z. Kolter, “Optnet: Differentiable optimization as a layer in neural networks,” in *International Conference on Machine Learning*. PMLR, 2017, pp. 136–145.

[59] A. Agrawal, B. Amos, S. Barratt, S. Boyd, S. Diamond, and J. Z. Kolter, “Differentiable convex optimization layers,” *Advances in Neural Information Processing Systems*, vol. 32, pp. 9562–9574, 2019.

[60] F. Sheikholeslami, A. Lotfi, and J. Z. Kolter, “Provably robust classification of adversarial examples with detection,” in *International Conference on Learning Representations*, 2020.

[61] K. Dvijotham, R. Stanforth, S. Gowal, T. A. Mann, and P. Kohli, “A dual approach to scalable verification of deep networks,” in *UAI*, vol. 1, no. 2, 2018, p. 3.

[62] E. Wong and Z. Kolter, “Provable defenses against adversarial examples via the convex outer adversarial polytope,” in *International Conference on Machine Learning*. PMLR, 2018, pp. 5286–5295.

[63] L. Li, X. Qi, T. Xie, and B. Li, “Sok: Certified robustness for deep neural networks,” *arXiv preprint arXiv:2009.04131*, 2020.

[64] S. Boyd, S. P. Boyd, and L. Vandenberghe, *Convex optimization*. Cambridge university press, 2004.

[65] N. P. Faíscà, V. Dua, and E. N. Pistikopoulos, “Multiparametric linear and quadratic programming,” pp. 3–23, 2007.

[66] Y. Ye and E. Tse, “An extension of karmarkar’s projective algorithm for convex quadratic programming,” *Mathematical Programming*, vol. 44, no. 1, pp. 157–179, May 1989.

[67] A. Bemporad and C. Filippi, “An algorithm for approximate multiparametric convex programming,” *Computational optimization and applications*, vol. 35, no. 1, pp. 87–108, 2006.

[68] I. Goodfellow, Y. Bengio, A. Courville, and Y. Bengio, *Deep Learning*. MIT Press Cambridge, 2016, vol. 1.

[69] O. Ben-Ayed and C. E. Blair, “Computational difficulties of bilevel linear programming,” *Operations Research*, vol. 38, no. 3, pp. 556–560, 1990.

[70] R. G. Jeroslow, “The polynomial hierarchy and a simple model for competitive analysis,” *Mathematical programming*, vol. 32, no. 2, pp. 146–164, 1985.

[71] B. Hanin and M. Sellke, “Approximating continuous functions by relu nets of minimal width,” *arXiv preprint arXiv:1710.11278*, 2017.

[72] P. Kidger and T. Lyons, “Universal approximation with deep narrow networks,” in *Conference on learning theory*. PMLR, 2020, pp. 2306–2327.

[73] K. Hornik, “Approximation capabilities of multilayer feedforward networks,” *Neural networks*, vol. 4, no. 2, pp. 251–257, 1991.

[74] B. Karg and S. Lucia, “Efficient representation and approximation of model predictive control laws via deep learning,” *IEEE Transactions on Cybernetics*, vol. 50, no. 9, pp. 3866–3878, 2020.

[75] A. Krizhevsky, I. Sutskever, and G. E. Hinton, “Imagenet classification with deep convolutional neural networks,” in *Proceedings of the International Conference on Neural Information Processing Systems*, vol. 1, Lake Tahoe, Nevada, USA, 2012, pp. 1097–1105.

[76] Y. Dong, Z. Deng, T. Pang, J. Zhu, and H. Su, “Adversarial distributional training for robust deep learning,” in *Advances in Neural Information Processing Systems*, vol. 33. Curran Associates, Inc., 2020, pp. 8270–8283.

[77] J. M. Danskin, *The theory of max-min and its application to weapons allocation problems*. Springer Science & Business Media, 2012, vol. 5.

[78] Z. Kolter and A. Madry, “Adversarial robustness: Theory and practice,” *Tutorial at NeurIPS*, p. 3, 2018.

- [79] A. Madry, A. Makelov, L. Schmidt, D. Tsipras, and A. Vladu, “Towards deep learning models resistant to adversarial attacks,” in *International Conference on Learning Representations*, 2018.
- [80] A. Chakraborty, M. Alam, V. Dey, A. Chattopadhyay, and D. Mukhopadhyay, “Adversarial attacks and defences: A survey,” *arXiv preprint arXiv:1810.00069*, 2018.
- [81] P. Ren, Y. Xiao, X. Chang, P.-Y. Huang, Z. Li, X. Chen, and X. Wang, “A survey of deep active learning,” *arXiv preprint arXiv:2009.00236*, 2020.
- [82] N. Qian, “On the momentum term in gradient descent learning algorithms,” *Neural networks*, vol. 12, no. 1, pp. 145–151, 1999.
- [83] R. W. Farebrother, *Linear least squares computations*. Routledge, 2018.
- [84] J. H. Park, Y. S. Kim, I. K. Eom, and K. Y. Lee, “Economic load dispatch for piecewise quadratic cost function using hopfield neural network,” *IEEE Transactions on Power Systems*, vol. 8, no. 3, pp. 1030–1038, Aug 1993.
- [85] S. Chatzivassileiadis, “Optimization in modern power systems,” *Lecture Notes. Tech. Univ. of Denmark. Available online: https://arxiv.org/pdf/1811.00943.pdf*, 2018.
- [86] “Power Systems Test Case Archive,” 2018, <http://labs.ece.uw.edu/pstca/>.
- [87] R. D. Zimmerman, C. E. Murillo-Sánchez, R. J. Thomas *et al.*, “MATPOWER: Steady-state operations, planning, and analysis tools for power systems research and education,” *IEEE Transactions on Power Systems*, vol. 26, no. 1, pp. 12–19, 2011.
- [88] S. Babaeinejadsarookolaei, A. Birchfield, R. D. Christie, C. Coffrin, C. DeMarco, R. Diao, M. Ferris, S. Fliscounakis, S. Greene, R. Huang *et al.*, “The power grid library for benchmarking AC optimal power flow algorithms,” *arXiv preprint arXiv:1908.02788*, 2019.
- [89] “pypower,” 2018, <https://pypi.org/project/PYPOWER/>.
- [90] J. Fortuny-Amat and B. McCarl, “A representation and economic interpretation of a two-level programming problem,” *Journal of the operational Research Society*, vol. 32, no. 9, pp. 783–792, 1981.

APPENDIX

Considering the original OPCC without removing the non-critical constraints:

$$\min_{\boldsymbol{x} \in \mathcal{R}^N} f(\boldsymbol{x}, \boldsymbol{\theta}) \quad (23)$$

$$\text{s.t. } a_i^T \boldsymbol{x} = b_i + c_i^T \boldsymbol{\theta}, \quad i = 1, \dots, p, \quad (24)$$

$$g_j(\boldsymbol{x}, \boldsymbol{\theta}) \leq e_j, \quad j = 1, \dots, m, m+1, \dots, m+q. \quad (25)$$

$$\underline{x}_k \leq x_k \leq \bar{x}_k, \quad k \in \mathcal{P}. \quad (26)$$

We solve the following problem for each inequality constraint $g_j, j = 1, \dots, m, m+1, \dots, m+q$ to identify if it is critical, i.e., whether it is active for at least one combination of the feasible input parameter $\boldsymbol{\theta}$ and \boldsymbol{x} :

$$\max_{\boldsymbol{\theta}, \boldsymbol{x}, i \in \mathcal{P}} g_j(\boldsymbol{\theta}, \boldsymbol{x}) - e_j \quad (27)$$

$$\text{s.t. } (24), (26), \quad \boldsymbol{\theta} \in \mathcal{D}$$

Recall that \mathcal{P} denotes the set of independent variables as in Sec. III. Constraints (24) and (26) describe the equality equations and enforce the feasibility of the variables in \mathcal{P} , which indicates the solution space of \boldsymbol{x} .

It should be clear that if the optimal value of (27) is non-positive for the j -th inequality constraint, i.e., $g_j \leq e_j$, then this inequality constraint is not critical in the sense that it can be removed without changing the optimal solution of OPCC for any input parameter in \mathcal{D} . We remark that if some inequality constraints g_j is linear w.r.t. \boldsymbol{x} and $\boldsymbol{\theta}$, then program (27) turns to be an LP, which can be efficiently solved global optimally by the existing solvers. Such condition holds for the DC-OPF problem studied in this work. For general convex g_j constraints, the program (27) is a non-convex optimization problem that can be NP-hard itself since we maximize with the convex objective.

The existing solvers may not be able to solving the problem global optimally. Therefore, any (sub-optimal) solution provided by the solvers is a lower bound on (27). We remark that if for some g_j , the obtained (sub-optimal) solution is positive, then such constraints is ensured to be critical and should not be removed. We leave the study on how to solve (27) global optimally for general convex constraints for future study. By solving (27) for all the inequality constraints, we obtain a set \mathcal{E} of critical inequality constraints whose optimal objectives are positive.

In [14], the authors adopt a similar idea to study the worst-case performance of DNNs in DC-OPF application, given the specification of DNN parameters. It is worth noticing that there exist several differences between these two problems. First, we consider the individual inequality constraint instead of the overall maximum constraints violation within the entire input-solution combinations. Second, we restrict the predicted variables in \mathcal{P} via (26). The benefits lie in that 1) it helps target each critical inequality constraints given an input parameter region, which is necessary for the further constraints calibration procedure, 2) it considers all possible occurrence of decision variables \mathbf{x} , which is the case of any possible output of DNNs, and 3) it indicates the effectiveness of the Sigmoid function in DNNs, which helps guarantee predicted variables' feasibility.

We provide the formulation of multiparameter quadratic program (mp-QP):

$$z(\boldsymbol{\theta}) = \min \quad \frac{1}{2} \mathbf{x}^T Q \mathbf{x} + \mathbf{d}^T \mathbf{x} \quad (28)$$

$$\text{s.t.} \quad a_i^T \mathbf{x} = b_i + c_i^T \boldsymbol{\theta}, \quad i = 1, \dots, p, \quad (29)$$

$$g_j^T \mathbf{x} \leq e_j + h_j^T \boldsymbol{\theta}, \quad j = 1, \dots, m, \quad (30)$$

$$\underline{x}_k \leq x_k \leq \bar{x}_k, \quad k \in \mathcal{P}, \quad (31)$$

$$\text{var.} \quad \mathbf{x} \in \mathcal{R}^N,$$

where $\mathbf{x} \in \mathcal{R}^N$ are the decision variables, $\boldsymbol{\theta} \in \mathcal{R}^M$ are the input parameters, $a_i, g_j \in \mathcal{R}^N, b_i, e_j \in \mathcal{R}, c_i, h_j \in \mathcal{R}^M$ are the coefficients of the equality and inequality constraints. $\mathbf{d} \in \mathcal{R}^N$ is a constant vector, Q is an $(N \times N)$ symmetric positive definite constant matrix. The above parametric mp-QP problem asks for the least objective for each input $\boldsymbol{\theta}$.

An applicable result from multiparametric programming that constrains the structure of the input-solution mapping $\Omega : \boldsymbol{\theta} \mapsto \mathbf{x}^*(\boldsymbol{\theta})$ is that $\mathbf{x}^*(\boldsymbol{\theta})$ is piece-wise continuous linear and the optimal objective $z(\boldsymbol{\theta})$ is piece-wise quadratic w.r.t. $\boldsymbol{\theta}$ [65].

Consider the following the linear constrained bi-level min-max problem:

$$\min_{\boldsymbol{\theta}} \max_{\mathbf{x}} \quad c^T \mathbf{x} \quad (32)$$

$$\text{s.t.} \quad \mathbf{A} \mathbf{x} \leq \mathbf{b} + \mathbf{F} \boldsymbol{\theta}, \quad (33)$$

$$\boldsymbol{\theta} \in \Theta, \quad (34)$$

where $\mathbf{A} \in \mathcal{R}^{p \times N}$, $\mathbf{b} \in \mathcal{R}^p$, $\mathbf{F} \in \mathcal{R}^{p \times M}$.

The above linear constrained bi-level program can be reformulated by introducing the sufficient and necessary KKT conditions [64] of the inner maximization problem. We present the reformulated program in the following:

$$\min_{\theta, \mathbf{x}, \mathbf{y}} \mathbf{c}^T \mathbf{x} \quad (35)$$

$$\text{s.t. } \mathbf{A}\mathbf{x} \leq \mathbf{b} + \mathbf{F}\theta, \text{ (Primal feasibility)} \quad (36)$$

$$\mathbf{A}^T \mathbf{y} = \mathbf{c}, \text{ (Stationarity)} \quad (37)$$

$$y_i \geq 0, \quad i = 1, \dots, p, \text{ (Dual feasibility)} \quad (38)$$

$$y_i(a_i^T \mathbf{x} - b_i - f_i^T \theta) = 0, \quad i = 1, \dots, p, \text{ (Complementary slackness)} \quad (39)$$

$$\theta \in \Theta. \quad (40)$$

Here a_i and f_i denote the i -th row of matrix \mathbf{A} and \mathbf{F} respectively. We remark that the nonlinear *Complementary slackness* condition in (39) can be reformulated to be mixed-integer linear using the Fortuny-Amat McCarl linearization [90]:

$$y_i \leq (1 - r_i)M, \quad a_i^T \mathbf{x} - b_i - f_i^T \theta \geq -r_i M. \quad (41)$$

Here the nonlinear the complementary slackness conditions are reformulated with the binary variable r_i and the large non-binding constant M for each $i = 1, \dots, p$. Therefore, problem (35)-(40) can be reformulated to be the mixed-integer linear program (MILP).

We first provide a toy example to demonstrate the non-uniqueness of the minimal supporting calibration region defined in Def. 2. Consider the following modified network flow problem:

$$\min \quad x_1^2 + x_2^2 + x_3^2 \quad (42)$$

$$\text{s.t. } 0 \leq x_1 \leq 90, \quad (43)$$

$$0 \leq x_2 \leq 90, \quad (44)$$

$$x_3 \leq 70, \quad (45)$$

$$x_1 + x_2 \leq 90, \quad (46)$$

$$x_2 + x_3 \leq 90, \quad (47)$$

$$x_1 + x_2 + x_3 = l. \quad (48)$$

Here l is the input load within $[0, 100]$ and x_1, x_2 , and x_3 can be seen as the network flow on the edges. Similar to the analysis in Sec. IV-B, the constraints (45)-(47) can be calibrated by at most 37.5% uniformly. However, such a calibration region is not the minimal one while forms the outer bound of it. Denote the calibration rate on (45)-(47) as (x, y, z) , it is easy to see that any combination such that $7x + 9y = 6$ and $z = 8/9 - y$ is the minimal supporting one.

We further provide the follow procedures to determine (one of) the minimal supporting region.

- Step 1. Solve (6)-(7) to obtain the maximal calibration rate Δ . Let $k = 1$.

- Step 2. For constraint g_k , solve

$$\min_{\boldsymbol{\theta}} \max_{x_i, i \in \mathcal{P}} \frac{\hat{e}_k - g_k(\boldsymbol{\theta}, \mathbf{x})}{|e_j|} \quad (49)$$

$$\text{s.t. } (2), (4), \quad \boldsymbol{\theta} \in \mathcal{D},$$

$$g_j(\boldsymbol{\theta}, \mathbf{x}) \leq \hat{e}_j, \forall j \in \mathcal{E}, \quad (50)$$

where $\hat{e}_k = e_k \times (1_{e_k \geq 0}(1 - \Delta) + 1_{e_k < 0}(1 + \Delta))$. Denote the optimal value of (49)-(50) as δ_k , which represent the maximal additional individual calibration rate of constraint g_k considering all other constraints' calibrations.

- Update \hat{e}_k to be $e_k \times (1_{e_k \geq 0}(1 - \Delta - \delta_k) + 1_{e_k < 0}(1 + \Delta + \delta_k))$ and proceed to the next iteration $k + 1$. Go to Step 2.

We remark that after each update of \hat{e}_k , the next g_{k+1} is studied on a tighter region described by $\{\hat{e}_j, j = 1, \dots, k\}$. After solving the programs for each g_k , one can easily see that the calibration region $\{\{\Delta + \delta_j\}_{j \in \mathcal{E}}\}$ is the minimal supporting calibration region.

We provide the details of applying *Danskin's Theorem* to solve the bi-level mixed-integer nonlinear problem (11)-(14) and discuss the relationship between the obtained solution and the global optimal one for general OPCC.

To solve such bi-level optimization problem, we optimize the upper-level variables $(W_i, b_i, i = 1, \dots, N_{\text{hid}})$ by gradient descent. This would simply involve repeatedly computing the gradient w.r.t. $(W_i, b_i, i = 1, \dots, N_{\text{hid}})$ for the object function, and taking a step in this negative direction. That is, we want to repeat the update

$$W_i := W_i - \alpha \cdot \nabla_{W_i} (\max_{\mathbf{x}} \nu_{|\mathcal{E}|}^f(W_i, b_i, \mathbf{x})), \quad (51)$$

$$b_i := b_i - \alpha \cdot \nabla_{b_i} (\max_{\mathbf{x}} \nu_{|\mathcal{E}|}^f(W_i, b_i, \mathbf{x})). \quad (52)$$

for each $i = 1, \dots, N_{\text{hid}}$. Here $\max_{\mathbf{x}} \nu_{|\mathcal{E}|}^f(W_i, b_i, \mathbf{x})$ denotes the maximum violation among the calibrated inequality constraints within the entire inputs domain \mathcal{D} , given the specific value of DNN parameters $(W_i, b_i, i = 1, \dots, N_{\text{hid}})$. Note that the inner function itself contains a maximization problem. We apply the *Danskin's Theorem* to compute the gradient of the inner term. It states that the gradient of the inner function involving the maximization term is simply given by the gradient of the function evaluated at this maximum. In other words, to compute the (sub)gradient of a function containing a $\max(\cdot)$ term, we need to simply: 1) find the maximum, and 2) compute the normal gradient evaluated at this point [76], [77]. Hence, the relevant gradient is given by

$$\nabla_{W_i} (\max_{\mathbf{x}} \nu_{|\mathcal{E}|}^f(W_i, b_i, \mathbf{x})) = \nabla_{W_i} \nu_{|\mathcal{E}|}^f(W_i, b_i, \mathbf{x}^*), \quad (53)$$

$$\nabla_{b_i} (\max_{\mathbf{x}} \nu_{|\mathcal{E}|}^f(W_i, b_i, \mathbf{x})) = \nabla_{b_i} \nu_{|\mathcal{E}|}^f(W_i, b_i, \mathbf{x}^*), \quad (54)$$

where

$$\mathbf{x}^* = \arg \max_{\mathbf{x}} \nu_{|\mathcal{E}|}^f(W_i, b_i, \mathbf{x}). \quad (55)$$

Here the optimal \mathbf{x}^* depends on the choice of DNN parameters $(W_i, b_i, i = 1, \dots, N_{\text{hid}})$. Therefore, at each iterative update of $(W_i, b_i, i = 1, \dots, N_{\text{hid}})$, we need to solve the inner maximization problem once. We use $\nu^{f,t}$ to denote the corresponding objective value $\nu_{|\mathcal{E}|}^f(W_i, b_i, \mathbf{x}^*)$.

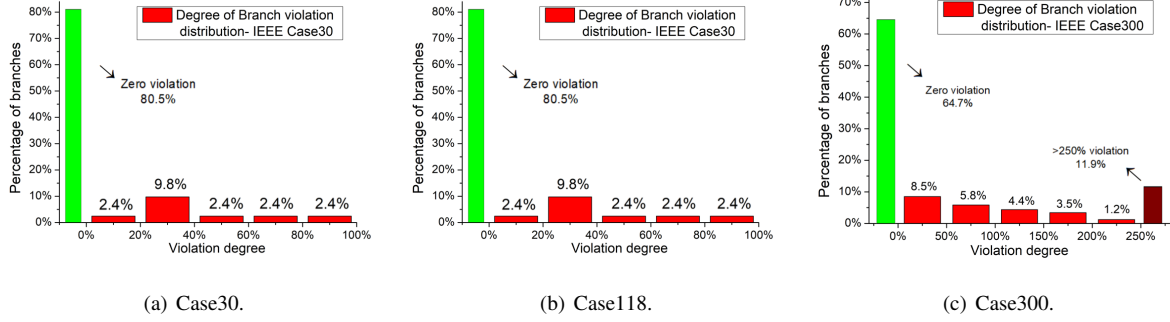


Fig. 4. Percentage and distribution of critical/non-critical transmission line of IEEE Case30, Case118, and Case300.

We remark that if the value of $\nu^{f,t} - \Delta$ is non-positive after some number of iterations for some DNN size, then the evaluated DNN size is capable of achieving universal feasibility w.r.t. the entire input domain \mathcal{D} . Otherwise if the value of $\nu^{f,t} - \Delta$ is always positive after t -th iteration with a large number of iterations t for some DNN size, the evaluated DNN size may not be able to preserve universal feasibility. Therefore, we need to increase the DNN size for better approximation ability.

It is worth noticing that the above result is based on the condition that we can obtain the global optimal solution of (11)-(14). However, one should note that for general OPCC 1) the inner maximization of (11)-(14) is indeed a non-convex mixed-integer nonlinear program due to the ReLU activations and the Sigmoid function at the output layer. The existing solvers, e.g., APOPT, YALMIP, or Gurobi, may not be able to provide the global optimal solution, meaning that for the given parameters of DNN ($W_i, b_i, i = 1, \dots, N_{\text{hid}}$), we actually obtain a lower bound on the maximum violation among all possible inputs $\theta \in \mathcal{D}$; 2) the iterative approach in (51)-(55) updating the DNN parameters of the outer problem characterizes the upper bound on such lower bound on the maximum violation from the inner problem given the DNN size. That is, for example if we can always solve the inner problem global optimally, the obtained value $\nu^{f,t}$ is the upper bound on ν^{f*} . If the inner problem only provides a lower bound on $\nu^{f*}|_{(W_i, b_i)}$ given the specification of DNN parameters, then the value of $\nu^{f,t}$ constructs the upper-lower bound on ν^{f*} . Though such a bound might not be tight, it indicates that it could be possible to achieve universal feasibility with such a DNN size if $\nu^{f,t} - \Delta \leq 0$. Otherwise if for some DNN size, the value of $\nu^{f*} - \Delta$ is always positive, then such evaluated DNN size may fail to guarantee universal feasibility.

A. Removing Non-Critical Inequality Constraints

1) *Removing Non-critical Branch Limits:* We propose the following program for each branch i to remove the non-critical branch limits given the entire load and generation space:

$$\max_{P_G, P_D} \nu_i - 1 \quad (56)$$

$$\text{s.t.} \quad \mathbf{A}_d P_D \leq b_d, \quad (57)$$

$$P_{Gi}^{\min} \leq P_{Gi} \leq P_{Gi}^{\max}, \forall i \in \mathcal{G} \setminus n_0, \quad (58)$$

$$P_G^{\text{slack}} = \sum_{i \in \mathcal{B}} P_{Di} - \sum_{i \in \mathcal{B} \setminus n_0} P_{Gi}, \quad (59)$$

$$\nu = |\tilde{\mathbf{X}}(\tilde{P}_G - \tilde{P}_D)|. \quad (60)$$

Here we assume the load domain $\mathcal{D} = \{P_D | \mathbf{A}_d P_D \leq b_d\}$ is restricted to a convex polytope described by matrix \mathbf{A}_d and vector b_d . (59) describes the power balance equation reformulated from the one in (18). (58) enforces the feasibility of non-slack generations, which is the case of the DNN outputs by applying the Sigmoid function at the output layer. (60) represents the normalized power flow level at each branch, where $\tilde{\mathbf{X}}$ is defined in (73) and $\nu \in \mathcal{R}^{|\mathcal{E}|}$.

We remark that problem (56)-(60) can be reformulated as two linear programmings to perform the inference of the absolute sign of power flows in (60):

$$\max_{P_G, P_D} / \min_{P_G, P_D} \tilde{\nu}_i \quad (61)$$

$$\text{s.t.} \quad (57) - (59),$$

$$\tilde{\nu} = \tilde{\mathbf{X}}(\tilde{P}_G - \tilde{P}_D). \quad (62)$$

If the optimal value of the above maximization (respectively minimization) problem is smaller or equal (respectively greater or equal) than 1 (respectively -1), then the optimal value of (61)-(62) is non-positive for some branch i . Therefore, such non-critical inequality constraint does not affect the feasible solution space such that it is always respected given any input load P_D and can be removed from the DC-OPF problem. By solving (61)-(62), we can derive the set \mathcal{E} of critical branch capacity constraints whose optimal objectives are positive.²¹

The percentage and distribution of the critical/non-critical transmission lines in IEEE Case30, Case118, and Case300 are shown in Fig. 4(a), Fig. 4(b), and Fig. 4(c) respectively. We observe that 80.5%, 76.9% and 64.7% of line limits in IEEE Case30, Case118, and Case300 are always inactive even under the worst-case scenarios.

2) *Removing Non-critical Slack Bus Generation Limits:* We provide the formulation to identify the critical slack generation limits given the entire load and generation space and the possible violation degree w.r.t. the upper and

²¹For the critical branch constraints not in \mathcal{E} , it is possible to encounter such load input and generation solution profiles using the DNN scheme with the Sigmoid function at output layer under the worst-case scenarios with which the power flow on branch i exceeds its transmission limit.

TABLE VII

RELATIVE SLACK BUS GENERATION LIMITS EXCEEDING AND THE PERCENTAGE OF CRITICAL INEQUALITY CONSTRAINTS.

Variants	IEEE Case30	IEEE Case118	IEEE Case300
Upper bound exceeding	2.1%	3.7%	7.5%
Lower bound exceeding	0.8%	0.9%	6.1%
Percentage of critical constraints	23.3%	23.9%	35.6%

lower bounds here.

$$\max_{P_G, P_D} \nu_{\text{slack}}^u \quad (63)$$

$$\text{s.t. } (57) - (59),$$

$$\nu_{\text{slack}}^u = \frac{P_{\text{slack}}^{\text{min}} - P_{\text{slack}}^{\text{max}}}{P_{\text{slack}}^{\text{max}} - P_{\text{slack}}^{\text{min}}}, \quad (64)$$

and

$$\max_{P_G, P_D} \nu_{\text{slack}}^l \quad (65)$$

$$\text{s.t. } (57) - (59),$$

$$\nu_{\text{slack}}^l = \frac{P_{\text{slack}}^{\text{max}} - P_G^{\text{slack}}}{P_{\text{slack}}^{\text{max}} - P_{\text{slack}}^{\text{min}}}, \quad (66)$$

respectively. Here (64) and (66) denote the (normalized) exceeding of slack bus generation exceeding its upper bound and lower bound, respectively. Therefore, if the optimal values of these proposed optimization problem is non-positive, such slack generation limit is non-critical and does not affect the load-solution feasible region.

We remark that problems (63)-(64), and (65)-(66) are indeed linear programs and can be efficiently solved by the state-of-the-art solvers such as CPLEX or Gurobi. We find that all three test cases could have both critical upper bound and lower bound limits, i.e., both (63)-(64) and (65)-(66) have positive optimal values. The (normalized) exceeding degrees on slack bus generation limits and the percentage of critical limits among all inequalities for the three test cases are reported in Table VII.

B. Maximum Constraints Calibration Magnitude

Recall that in DeepOPF+, the DNN is trained on the samples from OPF problems with adjusted constraints. However, if we reduce the limits too much, some load $P_D \in \mathcal{D}$ will become infeasible under the calibrated constraints and hence lead to invalid training data with poor generalization, though they are feasible for the original limits. Therefore, it is critical to determine the appropriate calibration range without reducing the supported load feasible

region. We propose the following bi-level optimization program to study such range with which the supported load feasible region \mathcal{D} is not reduced:

$$\min_{P_D} \max_{P_G} \nu^c \quad (67)$$

$$\text{s.t.} \quad (17), (20), (57)$$

$$\nu^c = \min\{..., \frac{P_{Tij}^{\max} - |PF_{ij}|}{P_{Tij}^{\max}}, ..., P_{\text{slack}}^u, P_{\text{slack}}^l\}, \quad (68)$$

where PF_{ij} denotes the power flow on branch $(i, j) \in \mathcal{E}$, calculated as in (70). P_{slack}^u and P_{slack}^l represent the relative upper and lower bounds redundancy on slack bus, given as

$$P_{\text{slack}}^u = (P_{\text{slack}}^{\max} - P_G^{\text{slack}})/k,$$

$$P_{\text{slack}}^l = (P_G^{\text{slack}} - P_{\text{slack}}^{\min})/k,$$

respectively, where $k = P_{\text{slack}}^{\max} - P_{\text{slack}}^{\min}$. Constraint (57) describes the convex polytope of P_D . Constraints (17) and (20) denote the feasibility of the corresponding P_G . Consider the inner maximization problem, the objective finds the maximum of the element-wise least redundancy of the limits at \mathcal{E} , which is the largest possible constraints calibration rate at each given P_D . The outer minimization problem hence finds the largest possible calibration rate among all $P_D \in \mathcal{D}$, and correspondingly, the supported load feasible region is not reduced. We remark that the inner maximization problem can be reformulated as a linear program (LP) by introducing a slack variable λ and a set of linear constraints, such that

$$\begin{aligned} \lambda &\leq \frac{P_{Tij}^{\max} - |PF_{ij}|}{P_{Tij}^{\max}}, \forall (i, j) \in \mathcal{E}, \\ \lambda &\leq (P_{\text{slack}}^{\max} - P_G^{\text{slack}})/k, \\ \lambda &\leq (P_G^{\text{slack}} - P_{\text{slack}}^{\min})/k. \end{aligned} \quad (69)$$

Here the first set of inequalities containing the absolute operations on power flows PF_{ij} can be reformulated to be linear. We apply the following procedures to solve the min-max bi-level problem: 1) dualize the innermost maximization problem to a minimization problem; 2) merge two minimization problems into a larger single-level optimization program. We remark that the above inner maximization problem is a primal feasible bounded LP (bounded feasible region of P_G). Therefore, its dual problem is feasible and bounded, with strong duality hold. After solving (67)-(68), we derive the maximum calibration rate for each test case, denoted as Δ . Numerical results are summarized in Table III.

C. Constraints Calibration in DC-OPF Problem

In DeepOPF+, we adjust the system constraints preventively during the training stage. Therefore, even with approximation errors of DNN, the predicted solutions are anticipated to be feasible at the test stage. In particular, we first calibrate the system constraints, i.e., the critical transmission line capacity limits and slack bus generator's

output limits, by an appropriate magnitude during the load sampling. As discussed in Sec. B, we reduce the line capacity limits by a certain rate $\eta_{ij} \geq 0$, i.e.,

$$|PF_{ij}| = \left| \frac{1}{r_{ij}} (\theta_i - \theta_j) \right| \leq P_{Tij}^{\max} \cdot (1 - \eta_{ij}), \quad \forall (i, j) \in \mathcal{E}, \quad (70)$$

where PF_{ij} and r_{ij} are the power flow and line reactance at branch (i, j) respectively. Set \mathcal{E} contains the critical branch limits that need to be calibrated. We refer to Sec. A for the detailed construction of \mathcal{E} . The above formulation (70) is exactly the dedicated description of the second set of constraints describing the branch limits in (18) for each branch $(i, j) \in \mathcal{E}$. The slack generation limits are also calibrated with $\xi \geq 0$, i.e.,

$$P_{\text{slack}}^{\min} + \xi \cdot k \leq P_G^{\text{slack}} \leq P_{\text{slack}}^{\max} - \xi \cdot k, \quad (71)$$

where P_{slack}^{\min} and P_{slack}^{\max} are the slack bus generation limits and $k = P_{\text{slack}}^{\max} - P_{\text{slack}}^{\min}$. The choice of η_{ij} and ξ is analyzed in details in Sec. B. Then, we train the DNN on a dataset created with calibrated limits to learn the corresponding load-to-generation ($P_D \mapsto \mathcal{S}$) mapping and evaluate its performance on a test dataset with the original limits. Thus, even with the inherent prediction error of DNN, the obtained solution can still remain feasible. We remark that during the training stage, the operational limits calibration does not reduce the feasibility region of the load inputs P_D in consideration. The constraints calibration only leads to the (sub)optimal solutions that are interior points within the original feasible region (the operational constraints are expected to be not binding). Note that the slack generation and the voltage phase angles can be obtained from (20) and (22) based on the predicted $\{\alpha_i\}_{i \in \mathcal{G} \setminus n_0}$ set-points. As benefits, the power balance equations in (18) are guaranteed to be held, and the size of the DNN model and the amount of training data and time can be reduced.

D. DNN Loss Function in DC-OPF Problem

The target of DNN training is to determine the value of W_i and b_i at each layer which minimize the average of the specified loss function \mathcal{L}_k among the training set, i.e.,

$$(W_i^*, b_i^*, i = 1, \dots, N_{\text{hid}}) = \arg \min_{W_i, b_i} \frac{1}{|\mathcal{K}|} \sum_{k=1}^{|\mathcal{K}|} \mathcal{L}_k,$$

where \mathcal{L}_k denotes the loss of training data k and $|\mathcal{K}|$ is the number of training data.

In this work, we adopt the supervised learning approach and design the loss function \mathcal{L} consisting of two parts to guide the training process. The first part is the sum of mean square error between the generated scaling factors $\hat{\alpha}_i$ and the reference ones α_i of the optimal solutions:

$$\mathcal{L}_{P_G} = \frac{1}{|\mathcal{G} - 1|} \sum_{i \in \mathcal{G} \setminus n_0} (\hat{\alpha}_i - \alpha_i)^2. \quad (72)$$

The second part consists of penalty terms related to the violations of the inequality constraints, i.e., line flow limits and slack bus generation:

$$\mathcal{L}_{\text{pen}} = \mathcal{L}_{\text{pen}}^{\text{line}} + \mathcal{L}_{\text{pen}}^{\text{slack}}, \quad (73)$$

which are given as:

$$\mathcal{L}_{pen}^{\text{line}} = \frac{1}{|\mathcal{E}|} \sum_{k=1}^{|\mathcal{E}|} \max \left(\left(\mathbf{X} \left(\tilde{P}_G - \tilde{P}_D \right) \right)_k^2 - 1, 0 \right),$$

$$\mathcal{L}_{pen}^{\text{slack}} = \frac{1}{|\mathcal{E}|} \max \left(\frac{P_G^{\text{slack}} - P_{\text{slack}}^{\text{max}}}{P_{\text{slack}}^{\text{max}} - P_{\text{slack}}^{\text{min}}}, 0 \right) + \frac{1}{|\mathcal{E}|} \max \left(\frac{P_{\text{slack}}^{\text{min}} - P_G^{\text{slack}}}{P_{\text{slack}}^{\text{max}} - P_{\text{slack}}^{\text{min}}}, 0 \right),$$

respectively. Here matrix \mathbf{X} is obtained from (21) by dividing each row of matrix $\tilde{\mathbf{B}}_{\text{line}} \tilde{\mathbf{M}}^{-1}$ with the value of corresponding line capacity. The first and second terms of $\mathcal{L}_{pen}^{\text{slack}}$ denote (normalized) the violations of upper bound and lower bound on slack generation, respectively. We remark that after the constraints calibration, the penalty loss is with respect to the adjusted limits. Note here the non-slack generations are always feasible as we predict the $(0, 1)$ scaling factors in (22). The total loss is a weighted sum of the two:

$$\mathcal{L} = w_1 \cdot \mathcal{L}_{P_G} + w_2 \cdot \mathcal{L}_{pen}, \quad (74)$$

where w_1 and w_2 are positive weighting factors representing the balance between prediction error and penalty. We apply the widely-used stochastic gradient descent (SGD) with momentum [82] method to update DNN's parameters $(W_i, b_i, i = 1, \dots, N_{\text{hid}})$ at each iteration.